Higgs boson contribution to the leading two-loop Yukawa corrections to $gg \rightarrow HH$

Joshua Davies[a], Go Mishima[b], Kay Schönwald[c],
Matthias Steinhauser[c], Hantian Zhang[c]

[a] *Department of Physics and Astronomy, University of Sussex, Brighton BN1 9QH, UK*

[b] *Department of Physics, Tohoku University, Sendai, 980-8578 Japan*

[c]*Institut für Theoretische Teilchenphysik, Karlsruhe Institute of Technology (KIT)
Wolfgang-Gaede Straße 1, 76128 Karlsruhe, Germany*

Abstract

We analytically compute two-loop Yukawa corrections to Higgs boson pair production in the high-energy limit. Such corrections are generated by an exchange of a Higgs boson between the virtual top quark lines. We propose two approaches to obtain expansions of the massive two-loop box integrals and show that precise results are obtained for transverse momenta of the Higgs bosons above about 150 GeV. We discuss in detail the computation of all 140 master integrals and present analytic results.

1 Introduction

Higgs boson pair production is a promising process which can provide experimental information about the Higgs boson self coupling (see, e.g., Ref. [1]). It is thus important to provide precise theoretical predictions of this process. The dominant contribution to Higgs boson pair production comes from gluon fusion, mediated by a top quark loop. There are a number of works in the literature in which QCD corrections to $gg \to HH$ have been considered. The NLO QCD corrections are known exactly [2–4], however, the numerical approach is quite computationally demanding. In practice it is therefore advantageous to construct approximations based on several expansions, valid in different regions of phase space [5–13]. A subsequent combination of the numerical approach with these expansions leads to fast and precise results which cover the whole phase space [14, 15]. At NNLO [16–21] and N³LO [22–26] only the large-m_t expansion has been considered. The to date most precise predictions have been obtained in Ref. [27] where a NNLO approximation has been constructed, based partly on exact and partly on large-m_t results.

Electroweak corrections are expected to be of the order of a few percent and thus they should be included in the theoretical description. In the Standard Model there are several couplings (gauge, Yukawa, Higgs boson self coupling) which are of different nature and can be treated separately. In this paper we take a first step towards the electroweak corrections and compute top quark Yukawa corrections originating from Higgs boson exchange in the top quark loop. More precisely, we consider diagrams like the one shown in Fig. 1. For this subclass only planar diagrams contribute and thus only planar integral families have to be considered.

Note that in the R_ξ gauge there are also other Yukawa corrections from the exchange of neutral and charged Goldstone bosons. They are not considered in this paper. Rather we concentrate on corrections with a virtual Higgs boson.

In the case of QCD corrections the top quark is the only massive particle in the loop. As additional scales, one has the Mandelstam variables s and t and the Higgs boson mass from the final-state particles. Electroweak corrections introduce additional masses in the propagators of the loop integrals, which increases the complexity significantly.

There are further classes of diagrams with a Higgs boson exchange. In contrast to the diagram in Fig. 1 they either involve Higgs boson self couplings (see Fig. 2(a)-(d)) or are one-particle reducible (see Fig. 2(e)-(h)). The results for the triangle diagrams in Fig. 2(a) can be obtained from the integral families discussed in this paper. Note that the diagram classes (b), (c) and (d) also involve non-planar contributions. Diagrams (e)-(h) are one-particle reducible and factorize into a product of one-loop integrals.

The master integrals which are computed in this paper are sufficient to compute the contributions from Figs. 2(a), (e), (f), (g) and (h). However, in this paper we concentrate on the two-loop box contribution of Fig. 1 and pursue the following goals:

- Develop a method to obtain high-energy approximations of two-loop four-point in-
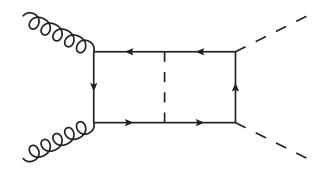
Figure 1: Sample Feynman diagram with a Higgs boson exchange in the top quark loop. Straight, dashed and curly lines represent top quarks, Higgs bosons and gluons, respectively.
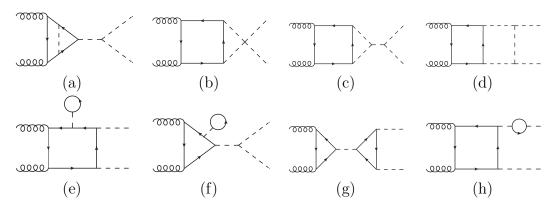

Figure 2: Diagrams with Higgs boson self coupling and one-particle reducible diagrams. These classes of diagrams are not considered in this paper.

tegrals where two different masses are present inside the loops.

- Provide details of the analytic computation of the master integrals which appear in the subclass of diagrams considered in this paper.

- Provide explicit analytic results for the master integrals in the high-energy limit.

The remainder of the paper is organized as follows: in the next section we introduce our notation and in Section 3 we outline the expansions which we apply to the Feynman diagrams. In Section 4 details of the computation of the amplitudes in terms of master integrals are provided. In Section 5 we provide a detailed description of the computation of the master integrals and numerical results of the form factors are are given in Section 6. We conclude in Section 7. In the appendix we present results for three-dimensional Mellin-Barnes integrals which enter our result.

2 Notation

The Mandelstam variables for the amplitude $g(q_1)g(q_2) \to H(q_3)H(q_4)$, with all momenta (q_i) defined to be incoming, are given by

$$s = (q_1 + q_2)^2 \,, \qquad t = (q_1 + q_3)^2 \,, \qquad u = (q_2 + q_3)^2 \,, \tag{1}$$

with

$$q_1^2 = q_2^2 = 0 \,, \qquad q_3^2 = q_4^2 = m_H^2 \,, \qquad s + t + u = 2m_H^2 \,. \tag{2}$$

It is convenient to introduce the scattering angle θ and the transverse momentum of the Higgs bosons in the center-of-mass frame, which are given by

$$
\begin{aligned}
p_T^2 &= \frac{ut - m_H^4}{s} \,, \\
t &= m_H^2 - \frac{s}{2}\left(1 - \cos\theta\sqrt{1 - \frac{4m_H^2}{s}}\right) \,.
\end{aligned}
\tag{3}
$$

Due to Lorentz and gauge invariance it is possible to define two scalar matrix elements $\mathcal{M}_1$ and $\mathcal{M}_2$ as

$$\mathcal{M}^{ab} = \varepsilon_{1,\mu}\varepsilon_{2,\nu}\mathcal{M}^{\mu\nu,ab} = \varepsilon_{1,\mu}\varepsilon_{2,\nu}\delta^{ab}\left(\mathcal{M}_1 A_1^{\mu\nu} + \mathcal{M}_2 A_2^{\mu\nu}\right) \,, \tag{4}$$

where a and b are adjoint colour indices and the two Lorentz structures are given by

$$
\begin{aligned}
A_1^{\mu\nu} &= g^{\mu\nu} - \frac{1}{q_{12}}q_1^\nu q_2^\mu \,, \\
A_2^{\mu\nu} &= g^{\mu\nu} + \frac{1}{p_T^2 q_{12}}\left(q_{33}q_1^\nu q_2^\mu - 2q_{23}q_1^\nu q_3^\mu - 2q_{13}q_3^\nu q_2^\mu + 2q_{12}q_3^\mu q_3^\nu\right) \,,
\end{aligned}
\tag{5}
$$

with $q_{ij} = q_i \cdot q_j$. The Feynman diagrams involving the Higgs boson self coupling only contribute to $A_1^{\mu\nu}$ and thus, it is convenient to decompose $\mathcal{M}_1$ and $\mathcal{M}_2$ into "triangle" and "box" form factors

$$
\begin{aligned}
\mathcal{M}_1 &= X_0\, s\left(\frac{3m_H^2}{s - m_H^2}F_{\text{tri}} + F_{\text{box1}}\right) \,, \\
\mathcal{M}_2 &= X_0\, s\, F_{\text{box2}} \,,
\end{aligned}
\tag{6}
$$

with

$$X_0 = \frac{G_F}{\sqrt{2}}\frac{\alpha_s(\mu)}{2\pi}T \,, \tag{7}$$

where $T = 1/2$, μ is the renormalization scale and G_F is the Fermi constant.

We define the perturbative expansion of the form factors as

$$F \;=\; F^{(0)} + \frac{\alpha_s(\mu)}{\pi} F^{(1,0)} + \frac{\alpha_t}{\pi} F^{(0,y_t)} + \cdots \,, \tag{8}$$

where α_t is given by

$$\alpha_t \;=\; \frac{\alpha\, m_t^2}{2\, s_W^2 m_W^2}\,. \tag{9}$$

α is the fine structure constant and $s_W^2 \equiv \sin^2\theta_W$ is the square of the sine of the weak mixing angle. Throughout this paper the strong coupling constant is defined with six active quark flavours. Note that the form factors are defined such that the one-loop colour factor T is contained in the prefactor X_0.

In this paper we only consider the contribution of the diagram class shown in Fig. 1 to F_{box1} and F_{box2}.

3   Asymptotic expansion

For the computation of the two-loop integrals we follow two approaches, which we describe in the following. For this purpose it is convenient to distinguish the mass of the final-state Higgs bosons (m_H^{ext}) from that of the Higgs boson which propagates in the loops (m_H^{int}). This means that for the process $gg \to HH$ we have the following dimensionful quantities: the Mandelstam variables s and t, and the masses m_t, m_H^{int} and m_H^{ext}. In our two approaches we assume the following hierarchies:

(A) $s, t \gg m_t^2 \gg (m_H^{\text{int}})^2, (m_H^{\text{ext}})^2,$

(B) $s, t \gg m_t^2 \approx (m_H^{\text{int}})^2 \gg (m_H^{\text{ext}})^2.$

In approach (A) we treat the inequality $m_t^2 \gg (m_H^{\text{int}})^2$ at the level of the integrand by applying the hard-mass expansion procedure as implemented in the program `exp` [28, 29]. For each Feynman diagram this leads to two subgraphs: the two-loop diagram itself and the one-loop diagram which contains all top quark lines. In the latter case the co-subgraph consists only of the Higgs boson propagator.

The two-loop subgraph is Taylor-expanded in m_H^{int} whereas the one-loop subgraph is expanded in the loop momentum of the co-subgraph, which is a one-loop vacuum integral with mass scale m_H^{int}. In addition, each subgraph is then expanded in m_H^{ext}, which is performed at the level of scalar integrals with the help of `LiteRed` [30, 31].

At this point one has to deal with one- and two-loop four-point integrals which only depend on the variables s, t and m_t. These integrals belong to the same set of topologies used in the calculation of the QCD corrections presented in Refs. [8, 9]; we are able to re-use those results here.

Approach (B) has the advantage that all expansions for the hierarchy $m_t^2 \approx (m_H^{\text{int}})^2 \gg (m_H^{\text{ext}})^2$ are simple Taylor expansions; no expansion by $\texttt{exp}$ is necessary. To implement the approximation $m_t^2 \approx (m_H^{\text{int}})^2$, we write the Higgs boson propagator in the form

$$
\begin{aligned}
i[D_h(p)]^{-1} &= (m_H^{\text{int}})^2 - p^2 \\
&= m_t^2(1 - \delta') - p^2 \,,
\end{aligned}
\tag{10}
$$

where $\delta' = 1 - (m_H^{\text{int}})^2/m_t^2$, and expand $D_h(p)$ in the limit $\delta' \to 0$ at the level of the integrand. The expansion in m_H^{ext} is then performed in the same way as for approach (A), described above. The remaining integrals are two-loop four-point integrals with massless legs, where all internal propagators have the mass m_t; this is a different set of integral topologies to those of the QCD corrections and approach (A).

In the final result, it is advantageous to introduce $\delta = 1 - m_H^{\text{int}}/m_t$. By making the replacement

$$
\delta' = \delta(1 + m_H^{\text{int}}/m_t) = \delta(2 - \delta) \,,
\tag{11}
$$

we obtain an expansion in δ which often has better convergence properties than the expansion in δ' (see also discussion at the end of Section 2 in Ref. [32]).

4 $gg \to HH$ amplitude and form factors

In this section we provide some details regarding how the two expansion approaches discussed in Section 3 are implemented. We generate the amplitude with $\texttt{qgraf}$ [33] and process the output with $\texttt{q2e}$ and $\texttt{exp}$ [28, 29] in order to generate $\texttt{FORM}$ [34] code for the amplitudes. This yields 6 one-loop diagrams and 60 two-loop diagrams.

As mentioned above, in approach (A) $\texttt{exp}$ identifies a one- and a two-loop sub-graph for each of the two-loop diagrams. The corresponding four-point integrals are expanded in m_H^{ext} using $\texttt{LiteRed}$ [30, 31] and then integration-by-parts (IBP) reduced to a set of master integrals using $\texttt{FIRE}$ [35]. These master integrals, which depend on s, t and m_t, are well-studied in the literature and the results of Refs. [8, 9] can be re-used here.

In approach (B), $\texttt{exp}$ does not perform any expansion but simply maps each diagram to a predefined integral family with massive final-state Higgs bosons and an internal Higgs boson propagator with mass m_H^{int}. These integrals are expanded in δ' at the level of the integrand by $\texttt{FORM}$, and the resulting scalar integrals are expanded in m_H^{ext} by $\texttt{LiteRed}$ and IBP reduced using $\texttt{FIRE}$. The number of master integrals is minimized using the $\texttt{FIRE}$ command $\texttt{FindRules}$, which equates identical integrals which belong to different integral families; this procedure yields a basis of 167 master integrals. We also apply $\texttt{FindRules}$ to the entire list of unreduced integrals, as discussed in Ref. [9]. Applying the IBP reduction tables to the equalities found here yields an additional 27 non-trivial relations between master integrals, thus we finally obtain a basis of 140 two-loop master integrals. We

Figure 3: The two-loop integral families which appear in expansion approach (B). The solid lines have mass m_t and the dotted external legs are massless. Variations of these families with permutations of the external legs also appear.

additionally perform the IBP reduction of a set of test integrals using `Kira` [36, 37]; here we also find a basis of 140 two-loop master integrals after minimizing between the different families.

These master integrals are four-point integrals with massless external legs, and all propagators have the mass m_t. Up to permutations of the external momenta, they belong to one of two integral families, shown in Fig. 3. The computation of these master integrals in the limit $s, t \gg m_t^2$ is described in Section 5.

The amplitudes for the two form factors are linear combinations of the master integrals, and we expand their coefficients to order $(m_H^{\text{ext}})^4$ and $(\delta')^3$. This expansion depth requires the IBP reduction of around 350,000 scalar integrals. We also pre-expand the coefficients in m_t and ϵ, and the final expansions of the form factors are obtained after inserting the m_t- and ϵ-expanded master integrals.

The freedom in the choice of basis for the master integrals can lead to some undesirable properties; the first is that the denominators of the coefficients of the master integrals in the reduction rules do not factorize in the dimensional regulator ϵ and the kinematic invariants and masses, s, t and m_t. The second is that the coefficients contain poles in ϵ, which imply that the master integrals need to be computed to higher orders in ϵ, to produce the finite contribution of the amplitude. The first point complicates the reduction and subsequent expansions of the amplitude, leading to poor computational performance. The second leads to unnecessarily difficult master integral computations involving functions and constants of higher transcendental weight which, ultimately, will cancel in the physical amplitude. We use an improved version of the program `ImproveMasters.m` [38] to find, for each family, a basis of master integrals for which both of these issues are avoided.

5   Fully massive two-loop box master integrals

The main purpose of this section is to provide details on the computation of the master integrals, which is based on differential equations [39–42]. The technically most challenging part is the computation of the boundary conditions which is described in Subsection 5.2.

5.1 Differential equations

The master integrals have a non-trivial dependence on two scaleless parameters $\hat{t} = t/s$ and $\hat{m}_t^2 = m_t^2/s$. We use `LiteRed` in combination with `FIRE` to derive linear systems of coupled differential equations with respect to each of the variables. In principle one can try to solve these sets of differential equations analytically, however the results are not expressible in terms of iterated integrals but rather involve more complicated structures like elliptic integrals. To obtain, nevertheless, precise and easy-to-evaluate results we follow the ideas of Ref. [8, 9] and evaluate the master integrals analytically in the high-energy expansion, i.e., for $m_t^2 \ll s, t$.

To construct the asymptotic expansion we insert a power-log ansatz for each master integral

$$I_n = \sum_{i=-2}^{i_{max}} \sum_{j=-4}^{j_{max}} \sum_{k=0}^{i+4} c_{ijk}^{(n)} \epsilon^i \hat{m}_t^{2j} \log^k(\hat{m}_t^2), \tag{12}$$

into the differential equation in the variable $\hat{m}_t^2$ and re-expand in ϵ and $\hat{m}_t$. Since there are no spurious poles in ϵ either in the physical amplitudes or the differential equations we can choose $i_{max} = 0$ for all master integrals. We have produced the expansion up to $j_{max} = 120$ for each of the master integrals, however the amplitudes contain spurious negative powers in m_t in the coefficients of the master integrals and additionally, one factor of m_t^2 is moved to the prefactor α_t. Thus the final expansion depth of the form factors for approaches (A) and (B) are $\hat{m}_t^{112}$ and $\hat{m}_t^{114}$, respectively.

After inserting the ansatz given in Eq. (12) for each master integral into the differential equation we can compare the coefficients of ϵ, $\hat{m}_t$ and $\log(\hat{m}_t^2)$ between the right- and left-hand side of the differential equation to obtain a system of linear equations for the expansion coefficients $c_{ijk}^{(n)}$. We use `Kira` together with `FireFly` [43, 44] to solve this system of equations in terms of a minimal set of boundary conditions, making sure to favour coefficients which belong to simpler master integrals and low ϵ expansion depth in the reduction. The main challenge is then to compute the remaining undetermined set of boundary conditions, which still depend on the second kinematic variable $\hat{t}$. We note that the set of boundary conditions required is independent of the value of j_{max}, thus the final expansion depth of the master integrals is limited only by the ability of `Kira` and `FireFly` to solve the large system of equations generated by high values of j_{max}. Deeper expansions than we have presented here are certainly possible, if required.

For the calculation of the $\hat{t}$ dependence of the boundary conditions in the limit $\hat{m}_t \to 0$ we use the methods developed in Refs. [8, 9, 45]. In particular, we use the method of expansion-by-regions [46, 47] to obtain integral representations for the required boundary coefficients. These are subsequently solved with the help of Mellin-Barnes integrals, either by analytically solving summations over residues or by high-precision numerical evaluations together with the `PSLQ` algorithm [48]. In the following section we will describe in detail how to obtain the integral representations of the asymptotic expansion in general

and show details of the calculation of a few examples explicitly.

We have performed numerical cross checks for all 140 master integrals with the help of FIESTA [49]. Using Euclidean kinematics, where both s and t are negative, we typically obtain six digits of agreement for the real-valued master integrals belonging to the integral families in Fig. 3. For these checks we use $m_t = 173$ GeV and set $s = t/2$ with $\sqrt{s} \geq 1200$ GeV. In the physical region, where $s > 0$ and $t \leq -s/2 < 0$, we find agreement for all 140 master integrals within the numerical uncertainty of FIESTA which provides between two and six significant digits. The lowest precision is obtained for the seven-line master integrals with dots, which are numerically very challenging. We have also performed consistency checks by inserting our analytic high-energy expansions into the system of t-differential equations and found that they are satisfied, order-by-order in m_t.

5.2   Boundary conditions: Mellin-Barnes approach

In this subsection, we demonstrate the Mellin-Barnes (MB) approach for the calculation of the boundary conditions for the $\hat{m}_t$-differential equations for the master integrals. We only consider the subset of master integrals for which the Euclidean region is defined by $S, T > 0$ and $U < 0$, where $S = -s, T = -t$ and $U = -u$. The remaining master integrals can then be found by crossing relations. The analytic continuation to the physical region is done at the end of the calculation.

5.2.1   Basics of Mellin-Barnes representations and template integrals

We start with a short review of the basics of MB representations and the usage of so-called "template integrals" in the asymptotic m_t expansion.[1] For a two-loop master integral with n lines we employ the following α representation,

$$
\mathcal{I}_n(S, T, U, m_t^2) \;=\; \int \prod_{j=1}^{2} \mathrm{d}l_j \, \frac{1}{D_1^{1+\delta_1} \cdots D_n^{1+\delta_n}} = \int_0^\infty \left(\prod_{i=1}^{n} \mathrm{d}\alpha_i \, \frac{\alpha_i^{\delta_i}}{\Gamma(1+\delta_i)} \right) \mathcal{U}^{-d/2} \, e^{-\mathcal{F}/\mathcal{U}},
$$
(13)

where $\mathcal{U}$ and $\mathcal{F}$ are Symanzik polynomials, δ_i are additional regulators associated with the denominators D_i, and the integration measure is chosen as

$$
\int \mathrm{d}l_j \;:=\; \frac{1}{\mathrm{i}\,\pi^{d/2}} \int \mathrm{d}^d l_j \quad \text{with} \;\; d = 4 - 2\,\epsilon.
$$
(14)

For later convenience, we further adopt the notation for the α-parameter measure as

$$
\int \mathrm{d}^n \alpha^\delta \;:=\; \int_0^\infty \prod_{i=1}^{n} \mathrm{d}\alpha_i \, \frac{\alpha_i^{\delta_i}}{\Gamma(1+\delta_i)} \, .
$$
(15)

---

[1]For a more detailed discussion of the MB method, we refer to [45].

We realize the asymptotic expansion in the high-energy region with the help of version 2.1 of the program `asy` [50]. Using as input

$$m_t^2 \sim \chi \,, \; S \sim 1 \,, \; T \sim 1 \,, \; U \sim 1 \quad \text{with } \chi \ll 1 \,, \tag{16}$$

`asy` provides the possible scalings of the α parameters in the asymptotic expansion; it provides a list of replacements $\alpha_i \to \chi^{n_i} \alpha_i$ which describe the different regions contributing to the asymptotic expansion.

In the "hard region" we have $m_t^2 \sim \chi$, while all α parameters scale as 1. Therefore, it corresponds to a simple Taylor expansion in m_t which can be realized via

$$\mathcal{I}_n^{(\text{hard})} \;\; = \;\; \sum_{k=0}^{\infty} \frac{\left(\chi \, m_t^2\right)^k}{k!} \frac{\partial^k}{\partial (m_t^2)^k} \mathcal{I}_n \bigg|_{m_t^2=0} \,. \tag{17}$$

The integrals on the r.h.s. can be reduced to known massless master integrals (see, e.g., Ref. [51, 52]) using IBP methods.

For the "soft regions", i.e. the regions in which at least one of the α parameters scales $\sim \chi$, we can expand the α representation of Eq. (13) according to the region's α-parameter scaling as[2]

$$\mathcal{I}_n^{(\text{soft})} \;\; = \;\; \sum_{r=1}^{R} \sum_{k=0}^{\infty} \int \mathrm{d}^n \alpha \, \delta \, \frac{(\chi)^k}{k!} \left[\frac{\partial^k}{\partial \chi^k} \left\{ \mathcal{U}_{(r)}^{-d/2} \exp\left(-\mathcal{F}_{(r)}/\mathcal{U}_{(r)}\right) \right\} \right]_{\chi=0} \,. \tag{18}$$

$\mathcal{U}_{(r)}$ and $\mathcal{F}_{(r)}$ are the Symanzik polynomials where χ has been introduced by applying the scaling of region r. Note that contrary to the hard region, which always starts at $\mathcal{O}(m_t^0)$, the soft regions can have different leading powers.

Taking the derivatives w.r.t. χ in Eq. (18) essentially produces the content of the curly brackets multiplied by polynomials in α_i, dimensionful quantities, the dimension d, and negative powers of $\mathcal{U}_{(r)}$. This allows us to define "shift operators" $\hat{\mathcal{S}}_r^k$ which reproduce the kth derivative in the region r without computing the derivative explicitly. Schematically, these shift operators can be written as

$$\hat{\mathcal{S}}_r^k\left(\{v_j\}, \{\alpha_i\}\right) \;\; = \;\; \sum_{\sigma} [\{v_j\} \, \text{monomial}]_\sigma \times \frac{[\{\alpha_i\} \, \text{polynomial}]_\sigma}{(\mathcal{U}_r)^{\rho_\sigma}} \,, \tag{19}$$

where σ runs over the various combinations of at most k^{th} order monomials constructed from $v_j \in \{m_t^2, d, S, T, U\}$, $\rho_\sigma \geq 0$ is an integer, and we have introduced the notation:

$$\mathcal{U}_r = \mathcal{U}_{(r)}\big|_{\text{coefficient of the leading term in } \chi} \,,$$
$$\mathcal{F}_r = \mathcal{F}_{(r)}\big|_{\text{coefficient of the leading term in } \chi} \,. \tag{20}$$

---

[2]Note that in general other scalings are possible for which Eq. (18) is not valid, however in the problem at hand we only encounter regions in which the α parameters scale as χ or as 1.

The χ-expansion of a region r can now be interpreted, not in terms of derivatives, but as the shifting of the indices of the single template integral of the region, $\mathcal{T}_r$. This template integral represents the leading integral in the region's χ-expansion and is given by

$$\mathcal{T}_r(\{\delta_i\}, \epsilon) \ := \ \int \mathrm{d}^n \alpha^\delta \, \mathcal{U}_r^{-d/2} \, e^{-\mathcal{F}_r/\mathcal{U}_r} \,. \tag{21}$$

We provide `Mathematica` expressions for all template integrals in the ancillary files [53]. The action of one possible term of the shift operators on the template integrals is given by:

$$\hat{\mathcal{S}}_r^k\Big(\{v_j\}, \{\alpha_i\}\Big) \circ \mathcal{T}_r\big(\{\delta_i\}, \epsilon\big) \ \supset \ \{v_j\} \text{ monomial} \times \frac{\prod_{i=1}^n \alpha_i^{\beta_i}}{(\mathcal{U}_r)^\rho} \, \mathcal{T}_r\big(\{\delta_i\}, \epsilon\big)$$

$$= \ \{v_j\} \text{ monomial} \times \left(\prod_{i=1}^n \mathcal{P}_{1+\delta_i}^{\beta_i} \right) \mathcal{T}_r\Big(\{\delta_i + \beta_i\}, \epsilon - \rho\Big) \,, \tag{22}$$

where $\beta_i \geq 0$ and $\rho \geq 0$ are integers and $\mathcal{P}_{1+\delta_i}^{\beta_i} = \Gamma(1+\delta_i+\beta_i)/\Gamma(1+\delta_i)$ is the Pochhammer function.

In this way, the higher-order χ-expansion terms for the master integrals without numerators[3] can be obtained from a single template integral per region. The full expansion of a master integral in the soft regions can therefore be written as

$$\mathcal{I}_n^{(\text{soft})} \ = \ \sum_{r=1}^R \left[1 + \sum_{k=1}^\infty \chi^k \hat{\mathcal{S}}_r^k\Big(\{v_j\}, \{\alpha_i\}\Big) \right] \circ \mathcal{T}_r\big(\{\delta_i\}, \epsilon\big) \,. \tag{23}$$

The MB representation of the template integrals can be obtained by means of direct integration over the α parameters and the application of Mellin-Barnes representations,

$$(x + y)^\lambda \ = \ \int_{-\mathrm{i}\infty}^{+\mathrm{i}\infty} \frac{\mathrm{d}z}{2\pi\mathrm{i}} \frac{\Gamma(-\lambda + z)\,\Gamma(-z)}{\Gamma(-\lambda)} \, x^z \, y^{\lambda-z} \,, \tag{24}$$

where the integration path has to be chosen in such a way as to separate the poles of the $\Gamma(\cdots + z)$ and $\Gamma(\cdots - z)$ factors. Note that the individual template integrals contain spurious poles in the regulators δ_i, which cancel in the sum of all soft regions.

5.2.2 Mellin-Barnes representations for master integrals with numerators

In the following we introduce a parametric method to directly obtain the MB representations for the boundary conditions of master integrals with numerators. Another method

---

[3]The shifting rule for master integrals with dotted propagators can be obtained directly from Eq. (22) by changing the δ indices.

would be to reduce master integrals with numerators to a basis of master integrals with only dots via IBP reductions. However in such a basis, deeper expansions in ϵ and m_t are often required due to the presence of spurious poles in the IBP relations.[4]

The numerators in the α representation can be introduced on the same footing as propagator denominators [31, 55] via

$$
\frac{1}{(D_i)^\lambda} = \begin{cases} \dfrac{1}{\Gamma(\lambda)} \displaystyle\int_0^\infty \mathrm{d}\alpha\, \alpha^{\lambda-1}\, e^{-D_i\,\alpha} & \text{for } \lambda > 0 \,, \\[2ex] (-1)^{|\lambda|}\, \dfrac{\partial^{|\lambda|}}{\partial\alpha^{|\lambda|}}\, e^{-D_i\,\alpha}\Big|_{\alpha=0} & \text{for } \lambda < 0 \,. \end{cases}
\tag{25}
$$

The α representation of the n-line master integral with m additional numerators can then be obtained as

$$
\begin{aligned}
\mathcal{I}_{n,m} &:= \int \prod_{j=1}^2 \mathrm{d}l_j\, \frac{N_1^{\lambda_1}\cdots N_m^{\lambda_m}}{D_1^{1+\delta_1}\cdots D_n^{1+\delta_n}} \\
&= \int_0^\infty \mathrm{d}^n\alpha^\delta\, \left[\left(\prod_{t=1}^m (-1)^{|\lambda_t|}\, \frac{\partial^{|\lambda_t|}}{\partial\alpha_{n+t}^{|\lambda_t|}}\right) \tilde{\mathcal{U}}^{-d/2}\, e^{-\tilde{\mathcal{F}}/\tilde{\mathcal{U}}}\right]_{\alpha_{n+1}=\cdots=\alpha_{n+m}=0} \\
&= \int_0^\infty \mathrm{d}^n\alpha^\delta\, \mathcal{U}^{-d/2}\, e^{-\mathcal{F}/\mathcal{U}}\, \hat{\mathcal{O}}^m\Big(\{v_j\}, \{\alpha_i\}\Big) \,,
\end{aligned}
\tag{26}
$$

where in our case we have $m = 1, 2$. In the second line, $\tilde{\mathcal{U}}$ and $\tilde{\mathcal{F}}$ are Symanzik polynomials in terms of $(n+m)$ α parameters, while in the last line $\mathcal{U}$ and $\mathcal{F}$ are those of Eq. (13) in terms of only n α parameters. The function $\hat{\mathcal{O}}^m$ comes from the derivatives in the second line; it has a similar form as the shift operators of Eq. (19). Note that in Eq. (26) no expansion in χ has been performed.

At this stage, having derived the n-dimensional α representation, we are ready to apply all the techniques developed for the n-line master integrals to Eq. (26). By performing the asymptotic expansions as described in Eq. (16), the resulting hard-region integral $\mathcal{I}_{n,m}^{(\text{hard})}$ can be solved in the same way as Eq. (17), and the integrals in the soft regions can be expressed as

$$
\begin{aligned}
\mathcal{I}_{n,m}^{(\text{soft})} &= \sum_{r=1}^R \int_0^\infty \mathrm{d}^n\alpha^\delta\, \mathcal{U}_r^{-d/2}\, e^{-\mathcal{F}_r/\mathcal{U}_r}\left[\sum_{k=0}^\infty \chi^k\, \hat{\mathcal{S}}_r^{k+m}\Big(\{v_j\}, \{\alpha_i\}\Big)\right] \\
&= \sum_{r=1}^R \left[\sum_{k=0}^\infty \chi^k\, \hat{\mathcal{S}}_r^{k+m}\Big(\{v_j\}, \{\alpha_i\}\Big)\right] \circ \mathcal{T}_r\big(\{\delta_i\}, \epsilon\big) \,,
\end{aligned}
\tag{27}
$$

where the action of the expanded shift operator $\hat{\mathcal{S}}_r^{k+m}$ follows the same rule as in Eq. (22), and the template integrals $\mathcal{T}_r$ are the same n-line integrals defined in Eq. (21). We emphasize that the shifts from operators $\hat{\mathcal{S}}_r^m$ yield the leading-order terms in the asymptotic m_t expansions of these master integrals with numerators.

---

[4] We notice a similar approach in [54] for numerical evaluations of quasi-finite master integrals.

Eq. (27) provides an algorithmic way to obtain the MB representations of master integrals with arbitrary numerators. Compared with using IBP reduction to change to a basis of master integrals without numerators, our method has the advantage of avoiding spurious higher-order poles in ϵ and m_t. Hence, one obtains a much more compact expression in terms of MB integrals, and the cancellation of δ_i-poles among different regions can be obtained more easily.[5]

5.2.3 Solving Mellin-Barnes integrals

In order to solve the MB representations derived in Eqs. (23) and (27), the first step is to fix the integration contour and perform analytic continuation and series expansions in the δ_i and ϵ regulators accordingly.[6] This step can be performed with the help of the package `MB.m` [56]. We now obtain a large number of multi-dimensional MB representations for complicated integrals, which requires a systematic approach for their calculation.

In general our method aims to find infinite sums of residues of the MB integrals, that are suitable for summation procedures. Such residue sum representations are passed to `EvaluateMultiSums.m` [57] and `HarmonicSums.m` [58] which internally use `Sigma.m` [59] for the analytic summation. This step is non-trivial, especially for multi-dimensional MB integrals, and it involves various supplementary techniques such as adding auxiliary scales, the T-expansion of MB integrals and ansatz fitting procedures, as well as numerical evaluation and the `PSLQ` algorithm. We will describe these methods by providing three examples in the following subsections.

In the following, we adopt the abbreviations

$$\Gamma[x_1, \ldots, x_n] := \prod_{i=1}^{n} \Gamma(x_i) , \quad \delta_{i_1 \ldots i_n} := \sum_{m=1}^{n} \delta_{i_m} , \quad \alpha_{i_1 \ldots i_n} := \sum_{m=1}^{n} \alpha_{i_m} , \quad (28)$$

and denote the Harmonic PolyLogarithms (HPLs) as $H(m_1, \ldots, m_n, x)$ (see Ref. [60] for their definition). We use $\log(x)$ and $H(0, x)$ interchangeably.

5.2.4 Example 1: three-line integral

We start by considering the three-line massive sunrise integral with massless external lines. The diagram is shown in Fig. 4, where solid and dotted lines denote massive and massless propagators, respectively. The Symanzik polynomials are given by

$$\begin{aligned} \mathcal{U} &= \alpha_1 \alpha_2 + \alpha_1 \alpha_3 + \alpha_2 \alpha_3 , \\ \mathcal{F} &= m_t^2 \left(\alpha_1 + \alpha_2 + \alpha_3 \right) \mathcal{U} , \end{aligned} \quad (29)$$

---

[5]Note that the complexity of Eq. (27) at $\mathcal{O}(\chi^k)$ is similar to the $\mathcal{O}(\chi^{m+k})$ expansions in Eq. (23).

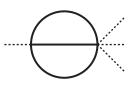[6]For details on the analytic continuation of multiple regulators, we refer to [45].

Figure 4: Three-line sunrise diagram with massless external lines. Solid internal lines represent massive scalar propagators. The dotted external lines indicate that the lines are massless.

and involve only one scale, m_t^2; hence there is no need to perform asymptotic expansion. We obtain a one-dimensional MB integral representation:

$$\mathcal{I}_3 \;=\; \int \frac{\mathrm{d}z_1}{2\pi\mathrm{i}} \left(m_t^2\right)^{-2\epsilon+1} \frac{\Gamma\left[-z_1, z_1-\epsilon+2, -z_1+\epsilon-1, z_1+1, z_1+1, z_1+\epsilon\right]}{\Gamma\left[2-\epsilon, 2z_1+2\right]}. \quad (30)$$

Since no expansion in m_t has to be performed the regulators δ_i are not required and have been dropped. We first fix the integration contour and the value of ϵ such that the left- and right-poles of the Gamma functions are separated by a straight line. In this case $\mathrm{Re}(z_1) = -1/7$ and $\epsilon = 1$ satisfy this condition. We then perform the analytic continuation $\epsilon \to 0$ such that we can expand the integrand in ϵ. These manipulations can be performed using MB.m [56], which yields

$$\mathcal{I}_3 \;=\; (m_t^2)^{1-2\epsilon} e^{-2\epsilon\gamma_E} \left(-\frac{3}{2\epsilon^2} - \frac{9}{2\epsilon} - \frac{21}{2} - \frac{5\pi^2}{12} + I^{(\mathrm{MB})} + \mathcal{O}(\epsilon) \right), \quad (31)$$

where the remaining MB integral

$$I^{(\mathrm{MB})} \;=\; \int_{-\frac{1}{7}-\mathrm{i}\infty}^{-\frac{1}{7}+\mathrm{i}\infty} \frac{\mathrm{d}z_1}{2\pi\mathrm{i}} \frac{\Gamma\left[-z_1-1, -z_1, z_1, z_1+1, z_1+1, z_1+2\right]}{\Gamma\left(2z_1+2\right)}. \quad (32)$$

In order to solve the integral $I^{(\mathrm{MB})}$ we can close the integration contour to the right and then sum the residues. We obtain:

$$I^{(\mathrm{MB})} \;=\; 4 + \frac{\pi^2}{6} + 2 \sum_{k=0}^{\infty} \binom{2k+1}{k}^{-1} \frac{(4k^2+8k+3)\left[S_1(k)-S_1(2k)\right] - 4(k+1)}{(2k+1)(2k+2)(2k+3)^2}, \quad (33)$$

where $S_i(n)$ denote harmonic sums, i.e., $S_i(n) = \sum_{k=1}^{n} \mathrm{sign}(i)^k / k^{|i|}$. As can be seen from the sum representation, the solution will be given by inverse binomial sums at infinity which have, for example, been studied in Ref. [61, 62]. However, their associated constants are not as well studied as those associated to the usual harmonic sums and thus a simplification of the final result is difficult; for this reason we proceed with a different method. The first step is to introduce a parameter into the sum and define

$$I^{(\mathrm{MB})}(\xi) \;=\; 4 + \frac{\pi^2}{6} + 2\xi \sum_{k=0}^{\infty} \xi^k \binom{2k+1}{k}^{-1} \frac{(4k^2+8k+3)\left[S_1(k)-S_1(2k)\right] - 4(k+1)}{(2k+1)(2k+2)(2k+3)^2}.$$

14

$$(34)$$

This allows us to find a generating function of the sum in Eq. (34) with the help of the command `ComputeGeneratingFunction` implemented in `HarmonicSums.m`. The result is expressed in terms of iterated integrals over the letters $\{1/x, \sqrt{4-x}\sqrt{x}\}$. Afterwards we rationalize the square-root valued letters with the command `SpecialGLToH` and take the limit $\xi \to 1$ to reconstruct $I^{\text{(MB)}}$ in Eq. (31). The result is given by

$$\lim_{\xi \to 1} I^{\text{(MB)}}(\xi) = \frac{\pi^2}{6} + \frac{27}{2} \left(\int_0^1 \frac{1}{1+\tau_1+\tau_1^2} d\tau_1 \right)^2 - 9 \left(\int_0^1 \int_0^{\tau_1} \frac{\tau_2}{\tau_1 \left(1+\tau_2+\tau_2^2\right)} d\tau_2 d\tau_1 \right).$$
$$(35)$$

We see that the solution can be written in terms of iterated integrals with cyclotomic letters [63]. They can be further reduced to known constants that are represented by multiple polylogarithms evaluated at the sixth roots of unity [64] which yields, for the ϵ-finite part of the massive sunrise diagram, the result

$$\mathcal{I}_3 = (m_t^2)^{1-2\epsilon} e^{-2\epsilon\gamma_E} \left(-\frac{3}{2\epsilon^2} - \frac{9}{2\epsilon} - \frac{21}{2} - \frac{11\pi^2}{12} + \psi^{(1)}\left(\tfrac{1}{3}\right) + \mathcal{O}(\epsilon) \right). \qquad (36)$$

Here $\psi^{(1)}\left(\tfrac{1}{3}\right)$ is the PolyGamma function that is related to the Clausen function by

$$\text{Cl}_2\left(\frac{\pi}{3}\right) = \frac{\psi^{(1)}\left(\tfrac{1}{3}\right)}{2\sqrt{3}} - \frac{\pi^2}{3\sqrt{3}}. \qquad (37)$$

When reconstructing analytic expressions from numerical evaluations using the `PSLQ` algorithm we therefore have to to use the following basis of constants as well as all possible products up to transcendental weight 4:

$$\left\{ 1,\, \sqrt{3},\, \log(2),\, \log(3),\, \pi,\, \psi^{(1)}\left(\tfrac{1}{3}\right),\, \zeta(3), \right.$$
$$\left. \text{Im}\left[\text{Li}_3\left(\tfrac{i}{\sqrt{3}}\right)\right],\, \text{Im}\left[\text{Li}_3\left(\tfrac{i\sqrt{3}}{4} + \tfrac{1}{4}\right)\right],\, \text{Li}_4\left(\tfrac{1}{2}\right) \right\}. \qquad (38)$$

5.2.5 Example 2: five-line integral

The second example is the five-line integral shown in Fig. 5. To fix the boundary conditions for the m_t differential equation for this integral we need to evaluate it including $\mathcal{O}(\epsilon^0, m_t^2)$; thus asymptotic expansion beyond the leading order in the m_t^2 expansion is required. The Symanzik polynomials for this master integral are given by

$$\mathcal{U} = (\alpha_2 + \alpha_3)(\alpha_1 + \alpha_4) + (\alpha_1 + \alpha_2 + \alpha_3 + \alpha_4)\alpha_5$$
$$\mathcal{F} = S\,\alpha_2\alpha_4\alpha_5 + T\,\alpha_1\alpha_3\alpha_5 + m_t^2\,(\alpha_1 + \alpha_2 + \alpha_3 + \alpha_4 + \alpha_5)\,\mathcal{U}, \qquad (39)$$
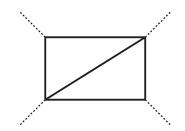
Figure 5: Five-line box diagram.

which involve three scales: S, T and m_t^2. By applying asymptotic expansions with `asy` according to the scaling in Eq. (16), we obtain 9 regions with the following α-parameter scalings:

$$(\alpha_1, \alpha_2, \alpha_3, \alpha_4, \alpha_5) \overset{\chi}{\sim} \underbrace{(0,0,0,0,0)}_{(0)}, \underbrace{(0,0,0,0,1)}_{(1)}, \underbrace{(0,0,1,1,0)}_{(2)}, \underbrace{(0,1,1,0,0)}_{(3)}, \underbrace{(0,1,1,0,1)}_{(4)},$$

$$\underbrace{(1,0,0,1,0)}_{(5)}, \underbrace{(1,0,0,1,1)}_{(6)}, \underbrace{(1,1,0,0,0)}_{(7)}, \underbrace{(1,1,1,1,0)}_{(8)}. \tag{40}$$

The scaling $(0,0,0,0,0)$ corresponds to the hard region, in which only $m_t^2 \sim \chi$ and all α parameters scale as $\alpha_i \sim \chi^0$. In the remaining eight regions a subset of the α parameters scale as $\alpha_j \sim \chi$.

Hard region: For the hard region, we proceed in the same way as Eq. (17). The leading term at $\mathcal{O}(m_t^0)$ can be obtained by setting $m_t = 0$, which corresponds to one of the known massless master integrals given in Refs. [65, 66]. For the sub-leading term at $\mathcal{O}(m_t^2)$, we first perform a Taylor expansion at the integrand level, and then perform an IBP reduction with `LiteRed` [30, 31] to reduce again to the set of known massless master integrals to obtain the final result.

Soft regions: For the soft regions, we apply the eight scalings from Eq. (40) to the Symanzik polynomials in Eq. (39), and expand the α representation to the sub-leading order in χ as described in Eq. (18). For region (1) we find, for example,

$$\mathcal{I}_5^{(\text{soft}),(1)} = \int d^5\alpha^\delta \, \mathcal{U}_1^{-d/2} \, e^{-\mathcal{F}_1/\mathcal{U}_1} \left[1 - \chi \left\{ m_t^2 \, \alpha_5 + \frac{d}{2} \frac{\alpha_{1234} \, \alpha_5}{\mathcal{U}_1} - S \frac{\alpha_2 \, \alpha_4 \, \alpha_{1234} \, (\alpha_5)^2}{(\mathcal{U}_1)^2} \right. \right.$$

$$\left. \left. - T \frac{\alpha_1 \, \alpha_3 \, \alpha_{1234} \, (\alpha_5)^2}{(\mathcal{U}_1)^2} \right\} + \mathcal{O}\left(\chi^2\right) \right], \quad (41)$$

with the expanded Symanzik polynomials

$$\mathcal{U}_1 = (\alpha_2 + \alpha_3)(\alpha_1 + \alpha_4) \, ,$$

16

$$\mathcal{F}_1 \;\; = \;\; S\,\alpha_2\alpha_4\alpha_5 + T\alpha_1\alpha_3\alpha_5 + m_t^2\left(\alpha_1 + \alpha_2 + \alpha_3 + \alpha_4\right)\mathcal{U}_1 \; . \tag{42}$$

Note that $\mathcal{U}_1$ is the coefficient of χ^0 and $\mathcal{F}_1$ is the coefficient of χ^1. The eight template integrals, which correspond to the leading contributions, can be extracted according to Eq. (21). They are represented by, at most, one-dimensional MB integrals.

The template integral for region 1 is given by

$$\mathcal{T}_{1,\{\delta_1,\delta_2,\delta_3,\delta_4,\delta_5\},\epsilon} \;\; = \;\; \int \frac{\mathrm{d}z_1}{2\pi\mathrm{i}} \frac{(m_t^2)^{-\delta_{1234}-2\epsilon}}{S^{\delta_5+1}} \left(\frac{T}{S}\right)^{z_1} \frac{\Gamma\left[\delta_{23} + \epsilon, \delta_{14} + \epsilon, \delta_2 - \delta_5 - z_1, -z_1\right]}{\Gamma\left[\delta_1 + 1, \delta_2 + 1, \delta_3 + 1, \delta_4 + 1\right]}$$

$$\times \frac{\Gamma\left[\delta_4 - \delta_5 - z_1, \delta_1 + z_1 + 1, \delta_3 + z_1 + 1, \delta_5 + z_1 + 1\right]}{\Gamma\left[\delta_{23} - \delta_5 + 1, \delta_1 + \delta_4 - \delta_5 + 1, \delta_5 + 1\right]} \; , \tag{43}$$

which is obtained from Eq. (21) through straightforward integration. The expansion in Eq. (41) can also be reinterpreted in terms of shift operators acting on this template integral:

$$\mathcal{I}_5^{\text{(soft)},(1)} \;\; = \;\; \left[1 + \chi \sum_{v\in\{m_t^2,d,S,T\}} \hat{\mathcal{S}}_1^1\left(v,\{\alpha_i\}\right)\right] \circ \mathcal{T}_{1,\{\delta_1,\delta_2,\delta_3,\delta_4,\delta_5\},\epsilon}$$

$$= \;\; \mathcal{T}_{1,\{\delta_1,\delta_2,\delta_3,\delta_4,\delta_5\},\epsilon} + \chi\Bigg[-m_t^2\,\mathcal{P}_{1+\delta_5}^1\,\mathcal{T}_{1,\{\delta_1,\delta_2,\delta_3,\delta_4,\delta_5+1\},\epsilon}$$

$$- \frac{d}{2}\,\mathcal{P}_{1+\delta_5}^1\bigg(\mathcal{P}_{1+\delta_1}^1\,\mathcal{T}_{1,\{\delta_1+1,\delta_2,\delta_3,\delta_4,\delta_5+1\},\epsilon-1} + \mathcal{P}_{1+\delta_2}^1\,\mathcal{T}_{1,\{\delta_1,\delta_2+1,\delta_3,\delta_4,\delta_5+1\},\epsilon-1}$$

$$+ \mathcal{P}_{1+\delta_3}^1\,\mathcal{T}_{1,\{\delta_1,\delta_2,\delta_3+1,\delta_4,\delta_5+1\},\epsilon-1} + \mathcal{P}_{1+\delta_4}^1\,\mathcal{T}_{1,\{\delta_1,\delta_2,\delta_3,\delta_4+1,\delta_5+1\},\epsilon-1}\bigg)$$

$$+ S\,\mathcal{P}_{1+\delta_5}^2\bigg(\mathcal{P}_{1+\delta_1}^1\mathcal{P}_{1+\delta_2}^1\mathcal{P}_{1+\delta_4}^1\,\mathcal{T}_{1,\{\delta_1+1,\delta_2+1,\delta_3,\delta_4+1,\delta_5+2\},\epsilon-2}$$

$$+ \mathcal{P}_{1+\delta_2}^2\mathcal{P}_{1+\delta_4}^1\,\mathcal{T}_{1,\{\delta_1,\delta_2+2,\delta_3,\delta_4+1,\delta_5+2\},\epsilon-2}$$

$$+ \mathcal{P}_{1+\delta_2}^1\mathcal{P}_{1+\delta_3}^1\mathcal{P}_{1+\delta_4}^1\,\mathcal{T}_{1,\{\delta_1,\delta_2+1,\delta_3+1,\delta_4+1,\delta_5+2\},\epsilon-2}$$

$$+ \mathcal{P}_{1+\delta_2}^1\mathcal{P}_{1+\delta_4}^2\,\mathcal{T}_{1,\{\delta_1,\delta_2+1,\delta_3,\delta_4+2,\delta_5+2\},\epsilon-2}\bigg)$$

$$+ T\,\mathcal{P}_{1+\delta_5}^2\bigg(\mathcal{P}_{1+\delta_1}^2\mathcal{P}_{1+\delta_3}^1\,\mathcal{T}_{1,\{\delta_1+2,\delta_2,\delta_3+1,\delta_4,\delta_5+2\},\epsilon-2}$$

$$+ \mathcal{P}_{1+\delta_1}^1\mathcal{P}_{1+\delta_2}^1\mathcal{P}_{1+\delta_3}^1\,\mathcal{T}_{1,\{\delta_1+1,\delta_2+1,\delta_3+1,\delta_4,\delta_5+2\},\epsilon-2}$$

$$+ \mathcal{P}_{1+\delta_1}^1\mathcal{P}_{1+\delta_3}^2\,\mathcal{T}_{1,\{\delta_1+1,\delta_2,\delta_3+2,\delta_4,\delta_5+2\},\epsilon-2}$$

$$+ \mathcal{P}_{1+\delta_1}^1\mathcal{P}_{1+\delta_3}^1\mathcal{P}_{1+\delta_4}^1\,\mathcal{T}_{1,\{\delta_1+1,\delta_2,\delta_3+1,\delta_4+1,\delta_5+2\},\epsilon-2}\bigg)\Bigg] \; . \tag{44}$$

At this point we use the MB representations derived for this region and perform the analytic continuation and expansion of the regulators $\delta_1,\ldots,\delta_5$ and ϵ, with the integration contour chosen at $\text{Re}(z_1) = -1/7$. As before, this is performed by MB.m and the left- and right-poles are separated by the straight contour line. The series expansion for the

individual regions yield both δ_i- and ϵ-poles. While the δ_i-poles have to cancel in the sum of all the soft regions for each master integral, the ϵ-poles cancel in the final sum of hard and soft regions for this diagram, since it is finite. The resulting one-dimensional MB integrals are solved by closing the integration contours either to the left or right and the subsequent summation of the residue sums using `Sigma.m` and `HarmonicSums.m` as described in the previous example.

Results: Solving the MB integrals in the soft regions and combining them with the hard region, we obtain the solution of the five-line integral of Fig. 5:

$$
\begin{aligned}
\mathcal{I}_5 \;=\; & \frac{1}{60(S+T)} \left\{ 20H(-1,\tfrac{T}{S}) \left[3\left(H(0,\tfrac{T}{S})^2 + \pi^2 \right) H\!\left(0,\tfrac{m_t^2}{S}\right) + 6\big(H(0,0,-1,\tfrac{T}{S}) \right.\right. \\
& + \zeta(3)\big) - 2H(0,\tfrac{T}{S})^3 - 3\left(2H(0,-1,\tfrac{T}{S}) + \pi^2 \right) H(0,\tfrac{T}{S}) \bigg] + 20H\!\left(0,\tfrac{m_t^2}{S}\right) \\
& \times \left(6\left(H(0,0,-1,\tfrac{T}{S}) + \zeta(3) \right) - 2H(0,\tfrac{T}{S})^3 - 3\left(2H(0,-1,\tfrac{T}{S}) + \pi^2 \right) H(0,\tfrac{T}{S}) \right) \\
& + 30\left(H(0,\tfrac{T}{S})^2 + \pi^2 \right) H\!\left(0,\tfrac{m_t^2}{S}\right)^2 - 120\zeta(3)H(0,\tfrac{T}{S}) + 15H(0,\tfrac{T}{S})^4 \\
& + 30\pi^2 H(0,\tfrac{T}{S})^2 + 60H(0,-1,\tfrac{T}{S}) H(0,\tfrac{T}{S})^2 + 120H(0,-1,-1,\tfrac{T}{S}) H(0,\tfrac{T}{S}) \\
& + 30H(-1,\tfrac{T}{S})^2 \left(H(0,\tfrac{T}{S})^2 + \pi^2 \right) - 120H(0,0,-1,-1,\tfrac{T}{S}) \\
& - 120H(0,0,0,-1,\tfrac{T}{S}) + 4\pi^4 \bigg\} + \frac{m_t^2}{ST} \left\{ 2H\!\left(0,\tfrac{m_t^2}{S}\right)^3 + \left(2 - 3H(0,\tfrac{T}{S}) \right) \right. \\
& \times H\!\left(0,\tfrac{m_t^2}{S}\right)^2 + \left(-2H(0,\tfrac{T}{S}) - 3\pi^2 - 8 \right) H\!\left(0,\tfrac{m_t^2}{S}\right) + H(0,\tfrac{T}{S})^3 \\
& + \left(6H(0,-1,\tfrac{T}{S}) + 3\pi^2 + 4 \right) H(0,\tfrac{T}{S}) + H(-1,\tfrac{T}{S})\left(-3H(0,\tfrac{T}{S})^2 - 3\pi^2 \right) \\
& - 6H(0,0,-1,\tfrac{T}{S}) - 14\zeta(3) - \pi^2 \bigg\} + \mathcal{O}(\epsilon, m_t^4) \,,
\end{aligned}
\tag{45}
$$

which is free from δ_i- and ϵ-poles.

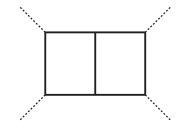### 5.2.6 Example 3: seven-line integral with two numerators

Figure 6: Seven-line double box diagram.

As a final example we consider the seven-line double box integral (see Fig. 6) with two additional numerators, which needs to be evaluated to $\mathcal{O}(\epsilon^0, m_t^0)$ for the boundary conditions.[7]

Alpha representation: We first derive the α representation of this "7+2"-line integral by the method presented in Eqs. (25)-(26) by treating the numerators on the same footing as the propagator denominators. The resulting Symanzik polynomials are given by

$$
\begin{aligned}
\tilde{\mathcal{U}} \ = \ & \alpha_6 \left(\alpha_3 + \alpha_4 + \alpha_5 + \alpha_7\right) + \left(\alpha_3 + \alpha_4 + \alpha_5\right) \alpha_8 + \alpha_7 \left(\alpha_3 + \alpha_4 + \alpha_5 + \alpha_8\right) \\
& + \left(\alpha_6 + \alpha_7 + \alpha_8\right) \alpha_9 + \left(\alpha_1 + \alpha_2\right) \left(\alpha_3 + \alpha_4 + \alpha_5 + \alpha_7 + \alpha_9\right) ,
\end{aligned}
$$

$$
\begin{aligned}
\tilde{\mathcal{F}} \ = \ & S \Big(\alpha_3 \big(\alpha_5 \left(\alpha_6 + \alpha_7 + \alpha_8\right) + \alpha_7 \left(\alpha_6 + 2\alpha_8\right) \big) + \big(\alpha_7 \alpha_8 - \alpha_4 \left(\alpha_6 + \alpha_7 + \alpha_8\right) \big) \alpha_9 \\
& \quad + \alpha_2 \big(\alpha_7 \left(\alpha_6 + 2\alpha_8\right) + \alpha_5 \left(\alpha_6 + \alpha_7 + 2\alpha_8\right) + \alpha_3 \left(\alpha_5 + \alpha_6 + 2\alpha_8\right) \\
& \quad + \alpha_4 \left(\alpha_6 + 2\alpha_8 - \alpha_9\right) + \left(\alpha_6 + 2\alpha_8\right) \alpha_9 \big) + \alpha_1 \big(\alpha_3 \alpha_5 - \left(\alpha_4 + \alpha_7\right) \alpha_9 \big) \Big) \\
& + T \Big(\alpha_1 \big(\alpha_4 \left(\alpha_7 - \alpha_8 - \alpha_9\right) - \alpha_8 \left(\alpha_3 + \alpha_5 + \alpha_7 + \alpha_9\right) \big) - \big(\alpha_4 \left(\alpha_2 + \alpha_6 + \alpha_7\right) \\
& \quad + \left(\alpha_4 - \alpha_7\right) \alpha_8 \big) \alpha_9 \Big) \\
& + m_t^2 \Big(\alpha_1 + \alpha_2 + \alpha_3 + \alpha_4 + \alpha_5 + \alpha_6 + \alpha_7 \Big) \tilde{\mathcal{U}} , \tag{46}
\end{aligned}
$$

and the seven-line Symanzik polynomials can be obtained from them:

$$
\mathcal{U} \ = \ \tilde{\mathcal{U}}\big|_{\alpha_8 = \alpha_9 = 0} , \qquad \mathcal{F} \ = \ \tilde{\mathcal{F}}\big|_{\alpha_8 = \alpha_9 = 0} . \tag{47}
$$

The α representation can be computed as

$$
\begin{aligned}
\mathcal{I}_{7,2} \ = \ & \int_0^\infty \mathrm{d}^7 \alpha^\delta \left(\frac{\partial}{\partial \alpha_8} \frac{\partial}{\partial \alpha_9} \tilde{\mathcal{U}}^{-d/2} e^{-\tilde{\mathcal{F}}/\tilde{\mathcal{U}}} \right) \bigg|_{\alpha_8 = \alpha_9 = 0} \\
= \ & \int_0^\infty \mathrm{d}^7 \alpha^\delta \, \mathcal{U}^{-d/2} e^{-\mathcal{F}/\mathcal{U}} \bigg(\hat{\mathcal{O}}^2 \left(d, \{\alpha_i\}\right) + \hat{\mathcal{O}}^2 \left(S, \{\alpha_i\}\right) + \hat{\mathcal{O}}^2 \left(T, \{\alpha_i\}\right) \\
& + \hat{\mathcal{O}}^2 \left(d^2, \{\alpha_i\}\right) + \hat{\mathcal{O}}^2 \left(S^2, \{\alpha_i\}\right) + \hat{\mathcal{O}}^2 \left(T^2, \{\alpha_i\}\right) + \hat{\mathcal{O}}^2 \left(d\,S, \{\alpha_i\}\right) \\
& + \hat{\mathcal{O}}^2 \left(d\,T, \{\alpha_i\}\right) + \hat{\mathcal{O}}^2 \left(S\,T, \{\alpha_i\}\right) \bigg), \tag{48}
\end{aligned}
$$

Note that no expansion is χ has yet been performed. The shift operators $\hat{\mathcal{O}}^2$ originate from the numerators of the integral, as explained in Eq. (26), and read:

$$
\hat{\mathcal{O}}^2 \left(d, \{\alpha_i\}\right) \ = \ \frac{d}{2\left(\mathcal{U}\right)^2} \, \alpha_7^2 ,
$$

$$
\hat{\mathcal{O}}^2 \left(S, \{\alpha_i\}\right) \ = \ \frac{S}{\left(\mathcal{U}\right)^3} \Big[2\alpha_{1267} \left(\alpha_2 \alpha_{3457} + \alpha_3 \alpha_7\right) \left(\left(2\alpha_{12} + \alpha_6\right) \alpha_{345} + \alpha_7 \left(\alpha_{56} + 2\alpha_{1234}\right)\right)
$$

---
[7]It corresponds to the integral $\mathtt{G}[4, \{1, 1, 1, 1, 1, 1, 1, -1, -1\}]$ in the ancillary file to this paper [53].

$$-\mathcal{U}\,\alpha_{27}\left((2\alpha_{12}+\alpha_6)\,\alpha_{345}+\alpha_7\left(\alpha_{56}+2\alpha_{1234}\right)\right)$$

$$-\mathcal{U}\left(2\alpha_{12}+\alpha_{67}\right)\left(\alpha_2\alpha_{3457}+\alpha_3\alpha_7\right)\Big]\,,$$

$$\hat{\mathcal{O}}^2\left(T,\{\alpha_i\}\right)\;=\;\frac{T}{\left(\mathcal{U}\right)^3}\Big[-2\alpha_1\alpha_{1267}\alpha_{3457}\left(\mathcal{U}+\alpha_4\alpha_7\right)+\alpha_1\mathcal{U}\alpha_{1267}\alpha_{3457}$$

$$+\left(\alpha_1-\alpha_7\right)\mathcal{U}\left(\mathcal{U}+\alpha_4\alpha_7\right)\Big]\,,$$

$$\hat{\mathcal{O}}^2\left(d^2,\{\alpha_i\}\right)\;=\;\frac{d^2}{4\left(\mathcal{U}\right)^2}\,\alpha_{3457}\,\alpha_{1267}\,,$$

$$\hat{\mathcal{O}}^2\left(S^2,\{\alpha_i\}\right)\;=\;-\frac{S^2}{\left(\mathcal{U}\right)^4}\left(\alpha_{34}\,\alpha_{126}+\alpha_{1234}\,\alpha_7\right)\left(\alpha_{45}\alpha_{126}+\alpha_{1456}\,\alpha_7\right)$$

$$\times\left(\alpha_{345}\left(2\,\alpha_{12}+\alpha_6\right)+\left(2\,\alpha_{1234}+\alpha_{56}\right)\alpha_7\right)\left(\alpha_3\alpha_7+\alpha_2\,\alpha_{3457}\right)\,,$$

$$\hat{\mathcal{O}}^2\left(T^2,\{\alpha_i\}\right)\;=\;\frac{T^2}{\left(\mathcal{U}\right)^4}\,\alpha_1\alpha_4\alpha_{3457}\,\alpha_{1267}\left(\mathcal{U}+\alpha_1\alpha_7\right)\left(\mathcal{U}+\alpha_4\alpha_7\right)\,,$$

$$\hat{\mathcal{O}}^2\left(d\,S,\{\alpha_i\}\right)\;=\;-\frac{d\,S}{2\left(\mathcal{U}\right)^3}\Big[\left(\left(\alpha_1\alpha_{47}+\alpha_4\alpha_{67}+\alpha_2\left(\alpha_4-\alpha_6\right)\right)\mathcal{U}\,\alpha_{3457}\right)$$

$$+\left(\alpha_2\left(\alpha_6\alpha_{45}+\alpha_3\alpha_{56}+\alpha_7\alpha_{56}\right)+\alpha_3\left(\alpha_5\alpha_{67}+\alpha_6\alpha_7\right)+\alpha_1\alpha_3\alpha_5\right)\alpha_{1267}\alpha_{3457}$$

$$-\left(\left(2\alpha_{12}+\alpha_6\right)\alpha_{345}+\alpha_7\left(2\alpha_{1234}+\alpha_{56}\right)\right)\alpha_{1267}\left(\alpha_2\alpha_{3457}+\alpha_3\alpha_7\right)\Big]\,,$$

$$\hat{\mathcal{O}}^2\left(d\,T,\{\alpha_i\}\right)\;=\;-\frac{d\,T}{2\left(\mathcal{U}\right)^3}\,\alpha_{3457}\,\alpha_{1267}\left(2\alpha_1\alpha_4\alpha_7+\alpha_{14}\mathcal{U}\right)\,,$$

$$\hat{\mathcal{O}}^2\left(S\,T,\{\alpha_i\}\right)\;=\;\frac{S\,T}{\left(\mathcal{U}\right)^4}\Big(\alpha_1\mathcal{U}\left(\alpha_1\alpha_{47}+\alpha_4\alpha_{67}+\alpha_2\left(\alpha_4-\alpha_6\right)\right)\alpha_{3457}\left(\alpha_4\alpha_7+\mathcal{U}\right)$$

$$+\alpha_1\left(\alpha_3\alpha_5\alpha_{12}+\alpha_7\alpha_{23}\alpha_{56}+\alpha_6\left(\alpha_2\alpha_{345}+\alpha_3\alpha_5\right)\right)\alpha_{1267}\alpha_{3457}\left(\alpha_4\alpha_7+\mathcal{U}\right)$$

$$+\alpha_1\alpha_4\alpha_7\alpha_{1267}\left(\alpha_2\alpha_{3457}+\alpha_3\alpha_7\right)\left(\alpha_7\alpha_{56}+\alpha_6\alpha_{345}-2\mathcal{U}\right)$$

$$-\alpha_4\alpha_{1267}\mathcal{U}\left(\alpha_2\alpha_{3457}+\alpha_3\alpha_7\right)\left(-\alpha_7\alpha_{56}-\alpha_6\alpha_{345}+2\mathcal{U}\right)\Big)\,,\tag{49}$$

with $\mathcal{U}=\alpha_{345}\,\alpha_{126}+\alpha_{123456}\,\alpha_7$. The absence of the remaining five possible shift operators $\{\hat{\mathcal{O}}^2(m_t^2),\hat{\mathcal{O}}^2(m_t^4),\hat{\mathcal{O}}^2(d\,m_t^2),\hat{\mathcal{O}}^2(S\,m_t^2),\hat{\mathcal{O}}^2(T\,m_t^2)\}$ is expected as the numerators are irreducible scalar products, which are free from m_t^2 terms.

Asymptotic expansions: With the representation in terms of seven α parameters for this "7+2"-line integral in hand, we can again apply the asymptotic expansions for the scaling of Eq. (16) to the seven-line Symanzik polynomials $\mathcal{U}$ and $\mathcal{F}$ (see Eq. (47)) as well as the shift operators in Eq. (49). The asymptotic expansion from `asy` yields the hard region and 13 soft regions with the following scalings:

$$(\alpha_1,\ldots,\alpha_7)\;\overset{\lambda}{\sim}\;\underbrace{(0,0,0,0,0,0,0)}_{0},\;\underbrace{(0,0,0,0,1,1,1)}_{1},\;\underbrace{(0,0,0,1,1,1,0)}_{2},\;\underbrace{(0,0,1,0,0,1,1)}_{3},$$

$$\underbrace{(0,0,1,1,1,1,1)}_{4}, \; \underbrace{(0,1,0,0,1,0,1)}_{5}, \; \underbrace{(0,1,1,0,0,0,1)}_{6}, \; \underbrace{(0,1,1,1,0,0,0)}_{7}, \; \underbrace{(0,1,1,1,1,0,1)}_{8},$$

$$\underbrace{(1,0,0,0,1,1,0)}_{9}, \; \underbrace{(1,1,0,0,1,1,1)}_{10}, \; \underbrace{(1,1,1,0,0,0,0)}_{11}, \; \underbrace{(1,1,1,0,0,1,1)}_{12}, \; \underbrace{(1,1,1,1,1,1,0)}_{13}.$$

$$(50)$$

For the hard region, we proceed in the standard way, i.e. we take the massless limit and perform IBP reductions to the known massless master integrals. For the 13 soft regions, we expand the α representation in Eq. (48) according to Eq. (27),

$$
\begin{aligned}
\mathcal{I}_{7,2}^{(\text{soft})} \;=\; & \sum_{r=1}^{13} \int_0^{\infty} \mathrm{d}^7\alpha\, \delta\, \mathcal{U}_r^{-d/2}\, e^{-\mathcal{F}_r/\mathcal{U}_r} \Bigg(\hat{\mathcal{S}}_r^2\left(d,\{\alpha_i\}\right) + \hat{\mathcal{S}}_r^2\left(S,\{\alpha_i\}\right) + \hat{\mathcal{S}}_r^2\left(T,\{\alpha_i\}\right) \\
& + \hat{\mathcal{S}}_r^2\left(d^2,\{\alpha_i\}\right) + \hat{\mathcal{S}}_r^2\left(S^2,\{\alpha_i\}\right) + \hat{\mathcal{S}}_r^2\left(T^2,\{\alpha_i\}\right) + \hat{\mathcal{S}}_r^2\left(d\,S,\{\alpha_i\}\right) \\
& + \hat{\mathcal{S}}_r^2\left(d\,T,\{\alpha_i\}\right) + \hat{\mathcal{S}}_r^2\left(S\,T,\{\alpha_i\}\right) + \mathcal{O}(\chi) \Bigg).
\end{aligned}
$$

$$(51)$$

The expanded shift operator $\hat{\mathcal{S}}_r^2$ is the leading term of the operator $\hat{\mathcal{O}}^2$ in Eq. (49) where the rth region scales according to Eq. (50). The 13 template integrals can be identified by $\mathcal{U}_r$ and $\mathcal{F}_r$ according to Eq. (21). By performing parametric integrations and Mellin transformations, we obtain up to three-dimensional MB representations for the template integrals. By applying the shift operators in Eq. (22) to Eq. (51), we obtain the MB representations of the soft regions.[8]

The next step is to perform an analytic continuation w.r.t. the eight regulators $\delta_1, \ldots, \delta_7$ and ϵ. We fix the integration contours at $\{\mathrm{Re}(z_1) = -1/7, \mathrm{Re}(z_2) = -1/11, \mathrm{Re}(z_3) = -1/17\}$ as straight lines. Then we perform the continuation with the MB.m package and expand the expression to order $\mathcal{O}(\delta_i^0)$ and $\mathcal{O}(\epsilon^0)$. This yields a large number of one-, two- and three-dimensional MB integrals; 2003, 515 and 14 respectively. In the following paragraphs, we will demonstrate our method to solve multi-dimensional MB integrals, focussing in particular on non-trivial examples which have a non-zero contribution from the contour-closing arc at infinity which must be taken into account.

Arc and residue sums: Here we start with a simple but non-trivial example which appears in our calculations, which demonstrates the importance of the arc contribution. The example is a one-dimensional scaleless MB integral with the integrand

$$f(z_2) \;=\; \frac{z_2^8\, \Gamma(-z_2)^2\, \Gamma(z_2)^2}{(z_2+1)^3\,(z_2+2)^3},$$

$$(52)$$

---

[8]An explicit example of applying the shift operators is shown in Eq. (44).

where the integration contour is fixed at $\text{Re}(z_2) = -1/11$. Cauchy's residue theorem states that

$$\int_{-\frac{1}{11}-i\infty}^{-\frac{1}{11}+i\infty} \frac{dz_2}{2\pi i} f(z_2) = -\sum_{k=0}^{\infty} \text{Res}_{z_2=k} [f(z_2)] - \int_{\text{arc}} \frac{dz_2}{2\pi i} f(z_2), \tag{53}$$

where the $(-)$ sign comes from the fact that we close the contour clockwise. One usually assumes that the arc contribution vanishes. However, this is not the case for Eq. (52). Closing the integration contour to the right and summing the residues we obtain

$$-\sum_{k=0}^{\infty} \text{Res}_{z_2=k} [f(z_2)] = -\sum_{k=0}^{\infty} \frac{3k^5(4+3k)}{(1+k)^4(2+k)^4}$$

$$= -18\zeta(3) - \frac{3\pi^2}{2} - \frac{21\pi^4}{10} + 240. \tag{54}$$

On the other hand, regularizing the integrand by multiplying with ξ^{z_2} and summing the residues we obtain

$$-\sum_{k=0}^{\infty} \text{Res}_{z_2=k} [\xi^{z_2} f(z_2)] = -\sum_{k=0}^{\infty} \xi^k \left(\frac{3k^5(4+3k)}{(1+k)^4(2+k)^4} + \frac{k^6}{(1+k)^3(2+k)^3} \log(\xi) \right)$$

$$\overset{\xi \to 1}{=} -18\zeta(3) - \frac{3\pi^2}{2} - \frac{21\pi^4}{10} + 241. \tag{55}$$

The same result can be found by precise numerical integration and employing the `PSLQ` algorithm. The difference between the two results in Eqs. (54) and (55) is the missing contribution from the arc in Eq. (53):

$$\int_{\text{arc}} \frac{dz_2}{2\pi i} f(z_2) = -1. \tag{56}$$

Therefore, in order to systematically take the arc contribution into account, we always rely on numerical integration of the MB integrals accompanied by the `PSLQ` algorithm to cross-check results obtained from the residue summations for scaleless MB integrals. However, the problem becomes more complicated when a non-vanishing arc contribution like Eq. (56) is nested in two-dimensional MB integrals involving the kinematic invariants T/S. In the following we will introduce a method which can deal with such situations.

Nested arc contribution: For two-dimensional MB integrals, we always first try to reduce their dimensionality using Barnes' lemmas as implemented in `barnesroutines.m` [67] and other simplification tricks. For the remaining two-dimensional MB integrals involving kinematic invariants and a nested arc contribution, we need a more careful analysis. Let us now consider two-dimensional MB integrals of the form

$$\int \frac{dz_1}{2\pi i} \frac{dz_2}{2\pi i} \left(\frac{T}{S} \right)^{z_1} \hat{\Gamma}(z_1) \hat{\Gamma}(z_2) \hat{\Gamma}(z_1, z_2), \tag{57}$$

22

where $\hat{\Gamma}$ denotes the product of Gamma functions with common integration variables. In our case we have two types of z_1 residues from the Gamma functions, which are given by

$$\begin{cases} \text{type 1: } z_1 = 0,\ 1,\ 2,\ \ldots \\ \text{type 2: } z_1 = g(z_2),\ g(z_2) + 1,\ g(z_2) + 2,\ \ldots \end{cases} \tag{58}$$

From the type 1 residues with integer z_1 we obtain

$$\begin{aligned} I_1 &= -\int \frac{\mathrm{d}z_2}{2\pi\mathrm{i}} \sum_{k_1=0}^{\infty} \mathrm{Res}_{z_1=k_1} \left(\frac{T}{S}\right)^{z_1} \hat{\Gamma}(z_1)\, \hat{\Gamma}(z_2)\, \hat{\Gamma}(z_1, z_2) \\ &= -\sum_{k_1=0}^{\infty} \left(\frac{T}{S}\right)^{k_1} \int \frac{\mathrm{d}z_2}{2\pi\mathrm{i}}\, \hat{F}(k_1, z_2)\, \hat{\Gamma}(z_2)\, \hat{\Gamma}(k_1, z_2), \end{aligned} \tag{59}$$

where $\hat{F}(k_1, z_2)$ denotes the resulting residue function. From the type 2 residues in Eq. (58), we have

$$\begin{aligned} I_2 &= -\int \frac{\mathrm{d}z_2}{2\pi\mathrm{i}} \sum_{k_1=0}^{\infty} \mathrm{Res}_{z_1=g(z_2)+k_1} \left(\frac{T}{S}\right)^{z_1} \hat{\Gamma}(z_1)\, \hat{\Gamma}(z_2)\, \hat{\Gamma}(z_1, z_2) \\ &= -\sum_{k_1=0}^{\infty} \int \frac{\mathrm{d}z_2}{2\pi\mathrm{i}} \left(\frac{T}{S}\right)^{g(z_2)+k_1} \hat{F}\big(g(z_2) + k_1, z_2\big)\, \hat{\Gamma}(z_2)\, \hat{\Gamma}\big(g(z_2) + k_1, z_2\big). \end{aligned} \tag{60}$$

We can then take the nested z_2 residues in Eqs. (59) and (60), which introduces a second infinite sum over k_2, and then perform the residue summations over both k_1 and k_2 with the help of `Sigma.m` and `EvaluateMultiSums.m`. However, this two-dimensional (k_1, k_2) residue summation will miss the arc contributions in the first type, given in Eq. (59), from scaleless one-dimensional MB integrals in z_2. The residue summation for the second type, given in Eq. (60), is correct, since the kinematic scale choice $0 < T/S < 1$ will suppress the asymptotic behaviour of the integrands and ensure that the arc contributions in Eq. (60) are vanishing. Instead of introducing another regulator into the two-dimensional MB integrals, which would increase the computational complexity significantly, we use precise numerical integration together with the PSLQ algorithm in order to find the correct results at fixed values of k_2. Clearly we can not compute the infinite sum in this way, so we introduce the method of T-expansion and ansatz fitting procedures to obtain the correct result for Eq. (57).

Ansatz fitting and T-expansions: The basic idea of this method is to start with an ansatz for the sum of MB integrals of the type given in Eq. (57) which contains rational functions and HPLs up to weight 4, and perform a series expansion in T to a finite power n. Then we expand Eqs. (59) and (60) up to $\mathcal{O}(T^n)$ by taking residues, and compute the remaining one-dimensional MB integrals. The result can then be fitted to

the series expansion of the ansatz; the fitting procedure consists of solving a system of linear equations to determine the unknown coefficients of the ansatz.

An ansatz which includes weight 4 functions is rather large, requiring a series expansion to a high power n to completely fix its coefficients. In practice, our experience shows that the arc does not contribute to the higher-transcendental-weight contributions, allowing us to limit the size of the ansatz and thus the required depth of the series expansions.

In the following, we demonstrate this idea with an explicit example that is present in our calculation. We have a two-dimensional MB expression I and perform the residue summation as described above. This leads to

$$
\begin{aligned}
I_{\text{sum}} &= \left(-\frac{4}{(x+1)^2} - \frac{12x}{(x+1)^2} - \frac{12x^2}{(x+1)^2} - \frac{4x^3}{(x+1)^2} - \frac{6H(-1,x)}{(x+1)^2} - \frac{4H(-1,x)}{x(x+1)^2} \right. \\
&\left. - \frac{2xH(-1,x)}{(x+1)^2} \right) \log(x) + I_{\text{sum}}^{(\text{high})},
\end{aligned}
\tag{61}
$$

where

$$
\begin{aligned}
I_{\text{sum}}^{(\text{high})} &= \left(-\frac{20x^3H(0,-1,x)}{(x+1)^2} - \frac{56x^2H(0,-1,x)}{(x+1)^2} - \frac{38xH(0,-1,x)}{(x+1)^2} + \frac{4H(0,-1,x)}{(x+1)^2} \right. \\
&\left. + \frac{8H(0,-1,x)}{x(x+1)^2} + \text{ weight 3 transcendental functions} \right) \log(x),
\end{aligned}
\tag{62}
$$

and $x = T/S$. $I_{\text{sum}}^{(\text{high})}$ contains functions of transcendental weight 3 and 4 which, in our calculation, are correctly computed by the residue sums. This suggests an ansatz which contains undetermined coefficients in front of functions only up to transcendental weight 2. Here we choose

$$
\begin{aligned}
I_{\text{ansatz}} &= \left(\frac{c_1}{(x+1)^2} + \frac{c_2 x}{(x+1)^2} + \frac{c_3 x^2}{(x+1)^2} + \frac{c_4 x^3}{(x+1)^2} + \frac{c_5 H(-1,x)}{x(x+1)^2} + \frac{c_6 H(-1,x)}{(x+1)^2} \right. \\
&\left. + \frac{c_7 x H(-1,x)}{(x+1)^2} + \frac{c_8 x^2 H(-1,x)}{(x+1)^2} + \frac{c_9 x^3 H(-1,x)}{(x+1)^2} \right) \log(x) + I_{\text{sum}}^{(\text{high})},
\end{aligned}
\tag{63}
$$

with the nine free parameters $c_1, \ldots, c_9$.

Using numerical integration and the `PSLQ` algorithm we can construct a series expansion of I which is given by

$$
\begin{aligned}
I_{\text{exp}} &= \left(4 - 40x - \frac{112x^2}{9} - \frac{1123x^3}{108} + \frac{148453x^4}{5400} - \frac{2409487x^5}{54000} + \frac{82787909x^6}{1323000} \right. \\
&- \frac{3017222321x^7}{37044000} + \frac{22492195259x^8}{222264000} - \frac{487063561297x^9}{4000752000} + \frac{1730875605497x^{10}}{12102274800} \\
&\left. + \mathcal{O}(x^{11}) \right) \log(x).
\end{aligned}
\tag{64}
$$

Note that here the arc contributions are included correctly. By performing a series expansion of Eq. (63) and comparing to Eq. (64) we obtain an over-determined system of linear equations with the solution

$$\{c_1 = -4,\ c_2 = -12,\ c_3 = -12,\ c_4 = -4,\ c_5 = 0,\ c_6 = 0,\ c_7 = 0,\ c_8 = 0,\ c_9 = 0\}. \quad (65)$$

After inserting the coefficients into Eq. (63) we finally obtain the true result for I which replaces Eq. (61).

Results: After solving all MB integrals and adding the result from the hard region, we derive the final solution of this "7+2"-line master integral

$$
\begin{aligned}
\mathcal{I}_{7,2} =\ & \frac{T}{4S^2} H\!\left(0, \tfrac{m_t^2}{S}\right)^4 + \frac{1}{T}\left\{ H(0, \tfrac{T}{S})\, H\!\left(0, \tfrac{m_t^2}{S}\right)^3 + \left(-\frac{3}{2} H(0, \tfrac{T}{S})^2 - \frac{\pi^2}{2}\right) H\!\left(0, \tfrac{m_t^2}{S}\right)^2 \right. \\
& + \left[H(0, \tfrac{T}{S})^3 + \left(6H(0, -1, \tfrac{T}{S}) + \pi^2\right) H(0, \tfrac{T}{S}) - 6H(0, 0, -1, \tfrac{T}{S}) \right] H\!\left(0, \tfrac{m_t^2}{S}\right) \\
& + H(-1, \tfrac{T}{S})\left[\left(-3H(0, \tfrac{T}{S})^2 - 3\pi^2\right) H\!\left(0, \tfrac{m_t^2}{S}\right) + 2H(0, \tfrac{T}{S})^3 \right. \\
& + \left. \left(8H(0, -1, \tfrac{T}{S}) + \frac{10\pi^2}{3}\right) H(0, \tfrac{T}{S}) - 8H(0, 0, -1, \tfrac{T}{S}) \right] - \frac{1}{4} H\!\left(0, \tfrac{m_t^2}{S}\right)^4 \\
& + \zeta(3)\left(8 - 8H(-1, \tfrac{T}{S})\right) - \frac{1}{4} H(0, \tfrac{T}{S})^4 + \left(-3H(0, -1, \tfrac{T}{S}) - \frac{\pi^2}{2}\right) H(0, \tfrac{T}{S})^2 \\
& - 8H(0, -1, -1, \tfrac{T}{S})\, H(0, \tfrac{T}{S}) + H(-1, \tfrac{T}{S})^2\left(-2H(0, \tfrac{T}{S})^2 - 2\pi^2\right) - \frac{1}{3}\pi^2 H(0, -1, \tfrac{T}{S}) \\
& + \left. 8H(0, 0, -1, -1, \tfrac{T}{S}) + 6H(0, 0, 0, -1, \tfrac{T}{S}) - \frac{5}{3} - \frac{\pi^2}{18} - \frac{19\pi^4}{180} + C_T \right\} \\
& + \frac{1}{S}\left\{ \zeta(3)\left(10H\!\left(0, \tfrac{m_t^2}{S}\right) - 8H(-1, \tfrac{T}{S}) - 4H(0, \tfrac{T}{S}) + 18\right) + H(0, \tfrac{T}{S})\, H\!\left(0, \tfrac{m_t^2}{S}\right)^3 \right. \\
& - \left(2H(0, \tfrac{T}{S})^2 + \frac{2\pi^2}{3}\right) H\!\left(0, \tfrac{m_t^2}{S}\right)^2 + \left[\frac{5}{3}H(0, \tfrac{T}{S})^3 + \left(6H(0, -1, \tfrac{T}{S}) + \frac{5\pi^2}{3}\right) H(0, \tfrac{T}{S}) \right. \\
& - \left. 6H(0, 0, -1, \tfrac{T}{S}) \right] H\!\left(0, \tfrac{m_t^2}{S}\right) + H(-1, \tfrac{T}{S})\left[\left(-3H(0, \tfrac{T}{S})^2 - 3\pi^2\right) H\!\left(0, \tfrac{m_t^2}{S}\right) \right. \\
& + \left. 2H(0, \tfrac{T}{S})^3 + \left(8H(0, -1, \tfrac{T}{S}) + \frac{10\pi^2}{3}\right) H(0, \tfrac{T}{S}) - 8H(0, 0, -1, \tfrac{T}{S}) \right] \\
& + \frac{1}{24} H\!\left(0, \tfrac{m_t^2}{S}\right)^4 - \frac{1}{2} H(0, \tfrac{T}{S})^4 - \left(2H(0, -1, \tfrac{T}{S}) + \pi^2\right) H(0, \tfrac{T}{S})^2 + \frac{2}{3}\pi^2 H(0, -1, \tfrac{T}{S}) \\
& - \left(8H(0, -1, -1, \tfrac{T}{S}) + 4H(0, 0, -1, \tfrac{T}{S})\right) H(0, \tfrac{T}{S}) - H(-1, \tfrac{T}{S})^2\left(2H(0, \tfrac{T}{S})^2 + 2\pi^2\right) \\
& + \left. 8H(0, 0, -1, -1, \tfrac{T}{S}) + 12H(0, 0, 0, -1, \tfrac{T}{S}) + \frac{5\pi^2}{18} - \frac{2}{3} - \frac{2\pi^4}{9} + C_S \right\} + \mathcal{O}(\epsilon, m_t^2),
\end{aligned}
$$

$$(66)$$

where the constants C_T and C_S originate from three-dimensional MB integrals which are discussed in Appendix A.

5.2.7 Crossing and analytic continuation

As stated above, we only calculate the boundary conditions for the subset of master integrals for which the Euclidean region is defined for $S, T > 0$ and $U < 0$. The boundary conditions for all other master integrals can be obtained by applying one of the five crossing relations:

$$T \to U \; ; \quad S \to U \; ; \quad S \leftrightarrow T \; ; \quad T \to U \, , \, S \to T \; ; \quad T \to S \, , \, S \to U \; . \tag{67}$$

While the rational dependence can be easily obtained via these replacements, the HPLs need analytic continuation.

Due to our choice of the Euclidean region we start with HPLs of the argument $x = T/S$, which are real in this region. To analytically continue to the physical region, we have to arrive at the argument $x' = -T/S = T/s = -x$. The transformation of HPLs to the negative argument is implemented in `HarmonicSums` and `HPL`. However, we have to take care to use the correct sign for the analytic continuation. We have $s = s + \mathrm{i}\varepsilon$, so $x = x + \mathrm{i}\varepsilon$ and therefore have to use the '+' sign for the analytic continuation which leads to

$$H(0, x) \;\; = \;\; H(0, x') + \mathrm{i}\pi \, . \tag{68}$$

Using `HarmonicSums` or `HPL` we can transform the argument of all occurring HPLs to the physical region. For example, we have

$$\begin{aligned}
H(0, -1, x) &= -H(0, 1, x'), \\
H(0, -1, -1, x) &= H(0, 1, 1, x') \, .
\end{aligned} \tag{69}$$

The analytic continuation of the HPLs after the application of the different crossings can be obtained in a similar manner, but require more involved transformations. For example, after the crossing $T \to U$ we end up with HPLs of the argument $y = -(1 + T/S + \mathrm{i}\varepsilon)$. We can map these HPLs back to argument x' by first applying the transformation $y \to -y = y'$ and afterwards $y' \to 1 - y' = x'$. The sign for the analytic continuation has to be chosen as '−' for the first and '+' for the second transformation. This results, for example, in

$$\begin{aligned}
H(0, -1, y) &= H(0, 1, x') - H(0, x')H(1, x') - \zeta(2), \\
H(0, -1, -1, y) &= -H(0, 0, 1, x') + H(0, x')H(0, 1, x') \\
&\quad - \frac{1}{2}H(0, x')^2 H(1, x') + \zeta(3) \, .
\end{aligned} \tag{70}$$

As a final example, let us look at the crossing $S \leftrightarrow T$. Here, we find HPLs of argument $w = S/T - \mathrm{i}\varepsilon$. We can map these HPLs back to argument x' by first applying the transformation $w \to 1/w = x$ and afterwards continue as for the first example. We find

$$H(0, -1, w) \;\; = \;\; H(0, 1, x') + \frac{1}{2}H(0, x')^2 - \frac{\pi^2}{3} + \mathrm{i}\pi\, H(0, x'),$$

$$H(0,-1,-1,w) = -H(0,1,1,x') + H(0,0,1,x') - H(0,x')H(0,1,x') - \frac{1}{6}H(0,x')^3$$
$$+ \frac{\pi^2}{2}H(0,x') + \zeta(3) - i\pi\left(H(0,1,x') + \frac{1}{2}H(0,x')^2 - \frac{\pi^2}{6}\right). \quad (71)$$

The analytic continuation for the other crossings can be derived analogously. In total we can express all 140 master integrals through the following set of HPLs:

$$\begin{aligned}
H\big(0,\tfrac{T}{s}\big) &= \log\big(\tfrac{T}{s}\big), \\
H\big(1,\tfrac{T}{s}\big) &= -\log\big(1-\tfrac{T}{s}\big), \\
H\big(0,1,\tfrac{T}{s}\big) &= \mathrm{Li}_2\big(\tfrac{T}{s}\big), \\
H\big(0,0,1,\tfrac{T}{s}\big) &= \mathrm{Li}_3\big(\tfrac{T}{s}\big), \\
H\big(0,1,1,\tfrac{T}{s}\big) &= -\mathrm{Li}_3\big(1-\tfrac{T}{s}\big) + \mathrm{Li}_2\big(1-\tfrac{T}{s}\big)\log\big(1-\tfrac{T}{s}\big) \\
&\quad + \tfrac{1}{2}\log\big(\tfrac{T}{s}\big)\log^2\big(1-\tfrac{T}{s}\big) + \zeta(3), \\
H\big(0,0,0,1,\tfrac{T}{s}\big) &= \mathrm{Li}_4\big(\tfrac{T}{s}\big), \\
H\big(0,0,1,1,\tfrac{T}{s}\big) &= \mathrm{S}_{2,2}\big(\tfrac{T}{s}\big), \\
H\big(0,1,1,1,\tfrac{T}{s}\big) &= -\mathrm{Li}_4\big(1-\tfrac{T}{s}\big) - \tfrac{1}{2}\mathrm{Li}_2\big(1-\tfrac{T}{s}\big)\log^2\big(1-\tfrac{T}{s}\big) + \tfrac{\pi^4}{90} \\
&\quad + \mathrm{Li}_3\big(1-\tfrac{T}{s}\big)\log\big(1-\tfrac{T}{s}\big) - \tfrac{1}{6}\log\big(\tfrac{T}{s}\big)\log^3\big(1-\tfrac{T}{s}\big). \quad (72)
\end{aligned}$$

While the expression in terms of HPLs is more convenient for analytic manipulations, the expressions in terms of polylogarithms ($\mathrm{Li}_n(x)$) and Nielsen polylogarithms ($S_{n,m}(x)$) might be more convenient for numerical evaluations, since many standard math libraries already contain implementations.

In the supplementary material to this paper [53] we provide the analytic results for all 140 master integrals.

6 Form factors for $gg \to HH$

The contribution to the form factors of $gg \to HH$ from diagrams of Fig. 1 is infrared finite and has only ultraviolet divergences. They are removed by renormalizing the top quark mass and Yukawa coupling in the leading order contributions. The counterterms are well known in the on-shell scheme, see, e.g., Ref. [68]. In this work it is sufficient to perform the renormalization in the $\overline{\mathrm{MS}}$ scheme. The corresponding mass counterterm is given by (see, e.g., Eq. (31) of Ref. [69])

$$m_t^0 = \overline{m}_t\left[1 + \frac{\alpha}{\pi s_W^2 \epsilon}\left(\frac{3}{32}\frac{\overline{m}_t^2}{m_W^2} + \frac{N_C}{4}\frac{\overline{m}_t^4}{m_W^2 m_H^2}\right)\right] = \overline{m}_t\left[1 + \frac{\alpha_t}{\pi\epsilon}\left(\frac{3}{16} + \frac{N_C}{2}\frac{\overline{m}_t^2}{m_H^2}\right)\right], \quad (73)$$

where α is the fine structure constant, $s_W \equiv \sin\theta_W$ is the sine of the weak mixing angle and $N_C = 3$. The second term inside the round brackets originates from the tadpole contribution[9] and is only provided for completeness; it is not used in this paper.

---

[9]For a recent improved prescription for the renormalization of tadpole contributions we refer to [70].
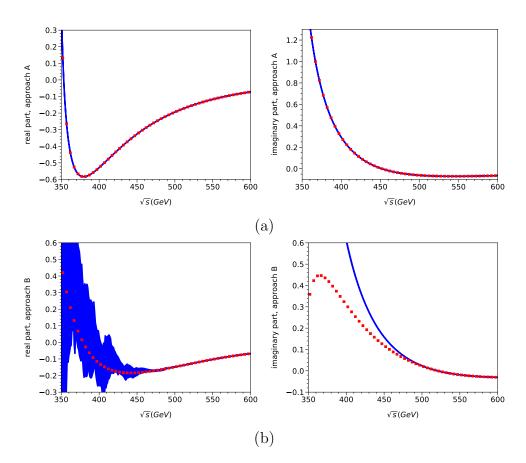
Figure 7: Real and imaginary parts of the seven-line master integral (see Fig. 6) for $p_T = 120$ GeV. Top: the line in the middle is massless; bottom: all lines are massive. Numerical results from `FIESTA` are shown in red; Padé results together with the corresponding uncertainty band are shown in blue.

The finite form factors F_{box1} and F_{box2} are expanded up to $(m_t^2)^{57}$ and m_H^4 in approach (A) and up to $(m_t^2)^{58}$, $(m_H^{ext})^4$ and δ^3 in approach (B). Note that one factor m_t^2 is collected in α_t (see Eq. (9)) such that the expansion up to $(m_t^2)^{56}$ and $(m_t^2)^{57}$ are available for the Padé method. We follow Ref. [71] and construct the so-called "pole distance re-weighted" Padé approximants and the corresponding uncertainties (see Section 4 of [71] for a detailed discussion), in which Padé approximants $[n/m]$ are included which satisfy

$$N_{\text{low}} \leq n + m \leq N_{\text{high}} \quad \text{and} \quad N_{\text{low}} \leq n + m - |n - m| \,. \tag{74}$$

For approach (A) we choose $\{N_{\text{low}}, N_{\text{high}}\} = \{50, 56\}$ and for approach (B) $\{N_{\text{low}}, N_{\text{high}}\} = \{51, 57\}$. Note that in [14] only terms up to $(m_t^2)^{16}$ are available. We observe that including more m_t expansion terms in the construction of the Padé approximations leads to a significant stabilization of the results, in particular for lower values of p_T. For the numerical analyses we choose $m_t = 173$ GeV, $m_H = 125$ GeV and set $\mu^2 = s$.

Before discussing the results for the physical form factors we apply our approximation method to the seven-line double box integral (see Fig. 6) where all internal lines are
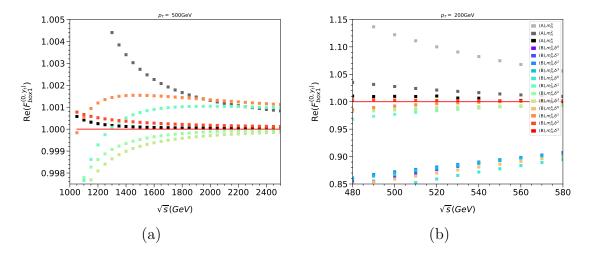
28

Figure 8: Real part of F_{box1} for different values of p_T and various expansion terms in m_H and δ.

massive. This is one of our master integrals, which we have expanded up to $(m_t^2)^{60}$. For this integral it is possible to obtain precise numerical results using FIESTA. In Fig. 7(b) we compare, for $p_T = 120$ GeV, the real and imaginary parts of the Padé method to the numerical results. For the Padé method we use $\{N_{\text{low}}, N_{\text{high}}\} = \{50, 60\}$, the same choice as we make for the form factors. For values of $\sqrt{s} \approx 500$ GeV and higher the Padé uncertainties are very small and we find perfect agreement between the Padé and FIESTA results. For lower $\sqrt{s}$ the Padé uncertainties in the real part grow. It is nevertheless interesting to see that the central values are close to the numerical results. On the contrary, for the imaginary part the Padé uncertainties remain small but there is a clear deviation from the exact result. This can be explained as follows: The integral we consider admits two- and three-particle cuts. For the latter $\sqrt{s} = 3m_t = 519$ GeV which is about the starting point for the deviations; the Padé method is not expected to be able to approximate the exact function below the cut, which we clearly see in the imaginary part in Fig. 7(b).

In Fig. 7(a) we show the analogous result for the seven-line master integral of approach (A) where middle line is massless. This integral only has cuts through two massive lines (and possibly also a massless line) and indeed, we observe good agreement of the Padé and FIESTA results, even close to the top quark pair threshold at $2m_t = 346$ GeV.

Let us now move to the form factors F_{box1} and F_{box2} and discuss the quality of the expansions in m_H and δ. For this purpose we fix p_T and plot various different depths. We normalize all curves to the highest-available depth of approach (B), which includes m_H^4 and δ^3.

In Fig. 8(a) the result is shown for the real part of F_{box1} for $p_T = 500$ GeV. The colours correspond to approach (B) and the results from approach (A) are shown in gray and black. The y axis spans a range below 1% and all approximations which include at least m_H^2 terms in approach (A) and m_H^2 and δ^1 terms in approach (B) are visible in the plot

and thus show a deviation well below the percent level.

In Fig. 8(b) we show results for $p_T = 200$ GeV and $\sqrt{s}$ values between 480 GeV and 580 GeV. For larger values of $\sqrt{s}$ the form factor crosses zero and the ratios inflate. Beyond the zero crossing the ratios are a similar size to those of Fig. 8(a). The result from approach (A) show a deviation of about 10% in case the Higgs mass is neglected. It reduced to below 5% after including the m_H^2 terms and is of order 1% after including also the quartic terms. The situation is similar for approach (B): Once quadratic terms in m_H and δ are include the deviation from 1 is below 5%. Including more expansion terms in m_H and δ further stabilizes the approximations.

We conclude that the inclusion of the quartic terms in m_H and cubic terms in δ provides an approximation to the (unknown) exact result below the percent level (see also Fig. 2 or Ref. [72] which shows a comparison for $gg \to ZH$).

Next we discuss the results for F_{box1} and F_{box2} for a range of values for the transverse momentum p_T. In Fig. 9 we show the real and imaginary parts of F_{box1} and F_{box2} for p_T between 120 GeV and 800 GeV. The colours correspond to the results from approach (B); here we also show the uncertainty band from the Padé method. The results from approach (A) are shown as faint uncertainty bands. They are only visible for small values of p_T, where one observes deviations between the two approaches.

Above $p_T = 200$ GeV the uncertainty from the Padé method is negligible. For $p_T = 150$ GeV differences between the approaches are only visible for the real part of F_{box2}. The situation is similar for $p_T = 120$ GeV for $\sqrt{s} \gtrsim 400$ GeV where the uncertainty bands are still small. Up to this value the results for F_{box1} and the imaginary parts of F_{box2} agree quite well. The real part of F_{box2} shows larger uncertainties for large values of $\sqrt{s}$ in approach (B); for approach (A), however, the uncertainties remain small. Note, that F_{box2} is numerically less important than F_{box1}.

Fig. 9 shows that both ways to treat the internal boson mass leads (within uncertainties) to equivalent physical results. In view of the discussion above we expect that approach (B) only approximates the unknown exact result down to $\sqrt{s} \approx 520$ GeV. However, approaches (A) and (B) agree for even smaller values of $\sqrt{s}$. It seems that the master integrals of approach (B) with non-analytic behaviour at the three-particle threshold are numerically suppressed.

In Fig. 10 we show the real and imaginary parts of F_{box1} and F_{box2} for fixed scattering angle $\theta = \pi/2$ for $\sqrt{s}$ between the top quark threshold and 1200 GeV. The solid curves represent Padé results and the dashed curves the expansions. We observe that the expansions start to diverge[10] for the real parts for $\sqrt{s} \approx 800$ GeV for approach (A) and for $\sqrt{s} \approx 1000$ GeV for approach (B). For the imaginary parts the numbers are 700 GeV and 600 GeV, respectively. Note, however, that the Padé results of approaches (A) and (B) are stable to fairly small values of $\sqrt{s}$. For $\sqrt{s} \gtrsim 500$ GeV the uncertainty bands are small

---

[10]In order to not overload the plots we only show the highest expansion terms in Fig. 10. The lower-order expansions show a similar behaviour.

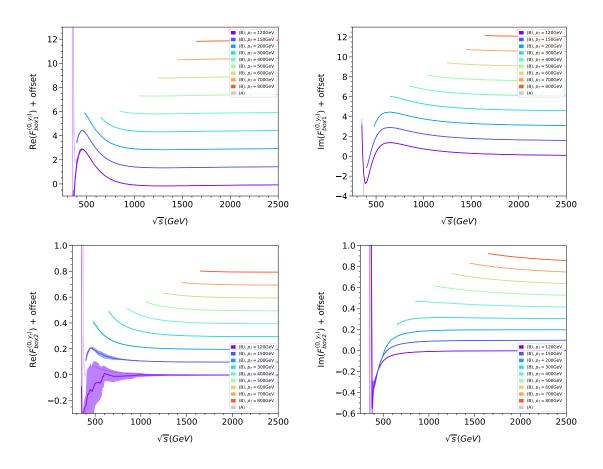Figure 9: Real and imaginary parts of F_{box1} and F_{box2} for fixed p_T. Note that an offset is applied such that the curves for the different p_T values are clearly separated. No offset is used for the lowest p_T value. For F_1 (F_2) we shift the subsequent p_T curves by 1.5 (0.1) in the positive y axis direction. The coloured curves and the corresponding bands correspond to approach (B). Results for approach (A) are only shown as faint uncertainty bands. For $p_T \geq 150$ GeV the central values of approach (A) and (B) agree.

and the two curves are on top of each other. For smaller values of $\sqrt{s}$ the uncertainty band of approach (B) becomes bigger whereas the ones of approach (A) remain small in accordance with the discussion of the three-particle threshold at the beginning of this section.

Let us finally perform a rough estimate of the numerical relevance of the contributions computed in this paper. For this purpose we only compare the real part of $F_{\text{box1}}^{(0,y_t)}$ to the corresponding contribution from the QCD corrections, $F_{\text{box1}}^{(1,0)}$. From Ref. [9] (see also Section 3.3 of Ref. [73]) we find that $F_{\text{box1}}^{(1,0)}$ is about $\mathcal{O}(1)$ if the scattering angle is fixed to $\theta = \pi/2$ and for $\sqrt{s}$ a few hundred GeV. This is also the case for $F_{\text{box1}}^{(0,y_t)}$ as can be seen from Fig. 10. For the pre-factors in Eq. (8) we have $\alpha_t/\alpha_s \approx 0.6$ and thus it might very well be that the electroweak corrections provide sizeable contributions to the Higgs pair cross section. Of course, we should emphasize that in this paper only a certain diagram
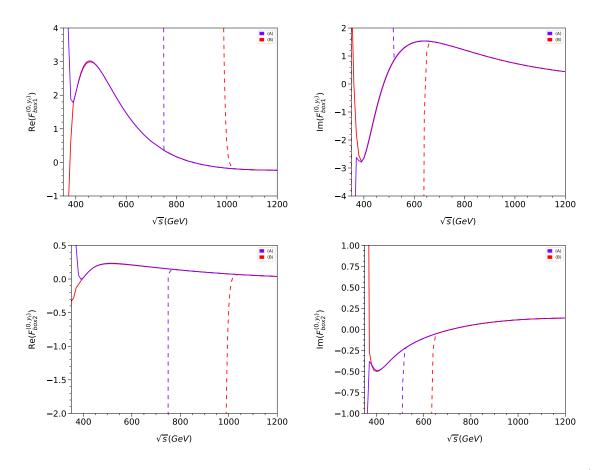
Figure 10: Real and imaginary parts of F_{box1} and F_{box2} for fixed scattering angle $\theta = \pi/2$.

class has been considered; in particular, no triangle diagrams are included. Furthermore for this estimate no interference contributions are taken into account.

7 Conclusions

In this paper we take the first step towards the electroweak corrections to Higgs boson pair production. We consider the subset of diagrams where a Higgs boson is exchanged between the top quarks. Effects from Higgs self couplings are neglected.

We are interested in analytic calculations of the form factors in the high-energy limit; we perform expansions in m_t^2/s, m_t^2/t and m_t^2/u taking into account up to about 60 expansion terms. We study two methods for the treatment of the internal massive Higgs boson, which is a new feature as compared to the QCD corrections. In our first approach we assume that it is small as compared to the top quark mass, whereas in the second approach it is assumed that the internal Higgs boson is of the same order of magnitude as the top quark mass. In both cases we perform expansions in the respective small parameters. For physical values of the mass parameters both expansion methods agree

at the percent level for smaller values of p_T and at the permille level for larger values.

The approach with a small internal Higgs boson leads to master integrals which have been computed in the context of QCD corrections. The other approach leads to 140 new master integrals. We describe in detail our approach to compute them analytically using differential equations and the Mellin Barnes method.

We supplement the expansion for small m_t by combinations of Padé approximations and the associated uncertainty estimates, which significantly increases the region of phase space where the analytic expansions can be used. We show that Padé approximants based on up to about 60 m_t^2 expansion terms provide excellent result down to $p_T = 150$ GeV and even for $p_T = 120$ GeV results with moderate uncertainties are obtained. On the basis of a scalar (master) integral we validate that the uncertainty estimate covers the exact result.

The methods discussed in this paper are not restricted to internal Higgs bosons. They can also be applied to internal gauge bosons and to other $2 \to 2$ processes mediated by a top quark loop and small external masses. For the subset of Feynman diagrams considered here only planar integrals contribute. The generalization to non-planar diagrams will be a challenge, however, we are optimistic that they can be treated using the methods developed in this paper.

Acknowledgements

A   Constants from three-dimensional MB integrals

The three-dimensional MB representations and the analytic expressions for the constants C_T and C_S present in the "7+2"-line integral are given by

$$
\begin{aligned}
C_T \; = \; & \int_{z_1 z_2 z_3} -\frac{2\Gamma\left[z_{12}+2, z_{12}+2, -z_3, z_3+1, z_3-z_1, z_{23}+2, -z_1, z_1+1, -z_2, -z_{23}-2, z_{123}+3\right]}{\Gamma\left[z_1+2, z_{12}+3, z_2+2z_3+3\right]} \\
& - \frac{4\Gamma\left[z_{12}+2, -z_{23}-1, -z_3, z_3+1, z_3-z_1, z_{23}+2, -z_1, z_1+1, -z_2, z_{12}+1, z_{123}+3\right]}{\Gamma\left[z_1+2, z_{12}+3, z_2+2z_3+3\right]} \\
& - \frac{4\Gamma\left[z_{12}+2, -z_{23}-1, -z_3, z_3+2, z_3-z_1, z_{23}+1, -z_1, z_1+1, -z_2, z_{12}+1, z_{123}+3\right]}{\Gamma\left[z_1+2, z_{12}+3, z_2+2z_3+3\right]}
\end{aligned}
$$

33

$$- \frac{2\Gamma\left[z_{12}+2, z_{12}+2, -z_3, z_3+1, -z_1+z_3+1, z_{23}+3, -z_1, z_1+1, -z_2, -z_{23}-3, z_{123}+3\right]}{\Gamma\left[z_1+2, z_{12}+3, z_2+2z_3+4\right]}$$

$$- \frac{2\Gamma\left[z_{12}+2, -z_{23}-2, -z_3, z_3+1, -z_1+z_3+1, z_{23}+3, -z_1, z_1+1, -z_2, z_{12}+1, z_{123}+3\right]}{\Gamma\left[z_1+2, z_{12}+3, z_2+2z_3+4\right]}$$

$$- \frac{6\Gamma\left[z_{12}+2, -z_{23}-2, -z_3, z_3+2, -z_1+z_3+1, z_{23}+2, -z_1, z_1+1, -z_2, z_{12}+1, z_{123}+3\right]}{\Gamma\left[z_1+2, z_{12}+3, z_2+2z_3+4\right]}$$

$$- \frac{2\Gamma\left[z_{12}+2, -z_{23}-3, -z_3, z_3+2, -z_1+z_3+2, z_{23}+3, -z_1, z_1+1, -z_2, z_{12}+1, z_{123}+3\right]}{\Gamma\left[z_1+2, z_{12}+3, z_2+2z_3+5\right]},$$

$$= \frac{5}{3} + \frac{\pi^2}{18} + \frac{88\pi^4}{405} - 8\zeta_3 - \frac{8\pi^2}{27}\psi^{(1)}\left(\tfrac{1}{3}\right) + \frac{2}{9}\left[\psi^{(1)}\left(\tfrac{1}{3}\right)\right]^2$$

$$\approx 6.890254528\ldots, \tag{75}$$

and

$$C_S = \int_{z_1 z_2 z_3} \frac{2\Gamma\left[z_{12}+2, z_{12}+2, -z_3, z_3+1, -z_1+z_3-1, z_{23}+1, -z_1, z_1+1, -z_2, -z_{23}-1, z_{123}+3\right]}{\Gamma\left[z_1+2, z_{12}+3, z_2+2z_3+2\right]}$$

$$- \frac{2\Gamma\left[z_{12}+2, -z_{23}-1, -z_3, z_3+1, z_3-z_1, z_{23}+2, -z_1, z_1+1, -z_2, z_{12}+1, z_{123}+3\right]}{\Gamma\left[z_1+2, z_{12}+3, z_2+2z_3+3\right]}$$

$$- \frac{2\Gamma\left[z_{12}+2, -z_{23}-1, -z_3, z_3+2, z_3-z_1, z_{23}+1, -z_1, z_1+1, -z_2, z_{12}+1, z_{123}+3\right]}{\Gamma\left[z_1+2, z_{12}+3, z_2+2z_3+3\right]}$$

$$- \frac{2\Gamma\left[z_{12}+2, z_{12}+2, -z_3, z_3+1, -z_1+z_3+1, z_{23}+3, -z_1, z_1+1, -z_2, -z_{23}-3, z_{123}+3\right]}{\Gamma\left[z_1+2, z_{12}+3, z_2+2z_3+4\right]}$$

$$- \frac{2\Gamma\left[z_{12}+2, -z_{23}-2, -z_3, z_3+1, -z_1+z_3+1, z_{23}+3, -z_1, z_1+1, -z_2, z_{12}+1, z_{123}+3\right]}{\Gamma\left[z_1+2, z_{12}+3, z_2+2z_3+4\right]}$$

$$- \frac{4\Gamma\left[z_{12}+2, -z_{23}-2, -z_3, z_3+2, -z_1+z_3+1, z_{23}+2, -z_1, z_1+1, -z_2, z_{12}+1, z_{123}+3\right]}{\Gamma\left[z_1+2, z_{12}+3, z_2+2z_3+4\right]}$$

$$- \frac{2\Gamma\left[z_{12}+2, -z_{23}-3, -z_3, z_3+2, -z_1+z_3+2, z_{23}+3, -z_1, z_1+1, -z_2, z_{12}+1, z_{123}+3\right]}{\Gamma\left[z_1+2, z_{12}+3, z_2+2z_3+5\right]},$$

$$= \frac{2}{3} - \frac{5\pi^2}{18} + \frac{649\pi^4}{1620} - 12\zeta_3 - \frac{20\pi^2}{27}\psi^{(1)}\left(\tfrac{1}{3}\right) + \frac{5}{9}\left[\psi^{(1)}\left(\tfrac{1}{3}\right)\right]^2$$

$$\approx 5.339941546\ldots, \tag{76}$$

where the integration contours are fixed at $\{\mathrm{Re}(z_1) = -1/7, \mathrm{Re}(z_2) = -1/11, \mathrm{Re}(z_3) = -1/17\}$.

The analytic result for C_T is obtained from a consistency condition obtained from the system of m_t-expanded t-differential equations for the 140 master integrals. On the other hand, for C_S we first perform various shifts of integration contours and analytic continuations to bring the three-dimensional MB integrals into a better form, which can be reduced to, at most, two-dimensional integrals in terms of only Gamma functions by the Barnes lemmas. The resulting MB integrals are the solved by the analytical summations and `PSLQ` algorithm. Note that it is straightforward to directly compute C_S and C_T numerically and obtain a precision of about ten digits, which is sufficient for practical applications.

References

[1] D. de Florian *et al.* [LHC Higgs Cross Section Working Group], [arXiv:1610.07922 [hep-ph]].

[2] S. Borowka, N. Greiner, G. Heinrich, S. P. Jones, M. Kerner, J. Schlenk, U. Schubert and T. Zirke, Phys. Rev. Lett. **117** (2016) no.1, 012001 Erratum: [Phys. Rev. Lett. **117** (2016) no.7, 079901] [arXiv:1604.06447 [hep-ph]].

[3] S. Borowka, N. Greiner, G. Heinrich, S. P. Jones, M. Kerner, J. Schlenk and T. Zirke, JHEP **1610** (2016) 107 [arXiv:1608.04798 [hep-ph]].

[4] J. Baglio, F. Campanario, S. Glaus, M. Mühlleitner, M. Spira and J. Streicher, arXiv:1811.05692 [hep-ph].

[5] S. Dawson, S. Dittmaier and M. Spira, Phys. Rev. D **58** (1998) 115012 [hep-ph/9805244].

[6] J. Grigo, J. Hoff, K. Melnikov and M. Steinhauser, Nucl. Phys. B **875** (2013) 1 [arXiv:1305.7340 [hep-ph]].

[7] G. Degrassi, P. P. Giardino and R. Gröber, Eur. Phys. J. C **76** (2016) no.7, 411 [arXiv:1603.00385 [hep-ph]].

[8] J. Davies, G. Mishima, M. Steinhauser and D. Wellmann, JHEP **1803** (2018) 048 doi:10.1007/JHEP03(2018)048 [arXiv:1801.09696 [hep-ph]].

[9] J. Davies, G. Mishima, M. Steinhauser and D. Wellmann, JHEP **01** (2019), 176 [arXiv:1811.05489 [hep-ph]].

[10] R. Bonciani, G. Degrassi, P. P. Giardino and R. Gröber, Phys. Rev. Lett. **121** (2018) no.16, 162003 [arXiv:1806.11564 [hep-ph]].

[11] R. Gröber, A. Maier and T. Rauh, arXiv:1709.07799 [hep-ph].

[12] X. Xu and L. L. Yang, arXiv:1810.12002 [hep-ph].

[13] G. Wang, Y. Wang, X. Xu, Y. Xu and L. L. Yang, Phys. Rev. D **104** (2021) no.5, L051901 [arXiv:2010.15649 [hep-ph]].

[14] J. Davies, G. Heinrich, S. P. Jones, M. Kerner, G. Mishima, M. Steinhauser and D. Wellmann, JHEP **11** (2019), 024 [arXiv:1907.06408 [hep-ph]].

[15] L. Bellafronte, G. Degrassi, P. P. Giardino, R. Gröber and M. Vitti, [arXiv:2202.12157 [hep-ph]].

[16] D. de Florian and J. Mazzitelli, Phys. Rev. Lett. **111** (2013) 201801 [arXiv:1309.6594 [hep-ph]].

[17] D. de Florian and J. Mazzitelli, Phys. Lett. B **724** (2013) 306 [arXiv:1305.5206 [hep-ph]].

[18] J. Grigo, K. Melnikov and M. Steinhauser, Nucl. Phys. B **888** (2014) 17 [arXiv:1408.2422 [hep-ph]].

[19] J. Grigo, J. Hoff and M. Steinhauser, Nucl. Phys. B **900** (2015) 412 [arXiv:1508.00909 [hep-ph]].

[20] J. Davies, F. Herren, G. Mishima and M. Steinhauser, JHEP **05** (2019), 157 [arXiv:1904.11998 [hep-ph]].

[21] J. Davies, F. Herren, G. Mishima and M. Steinhauser, JHEP **01** (2022), 049 [arXiv:2110.03697 [hep-ph]].

[22] M. Spira, JHEP **10** (2016), 026 [arXiv:1607.05548 [hep-ph]].

[23] M. Gerlach, F. Herren and M. Steinhauser, JHEP **11** (2018), 141 [arXiv:1809.06787 [hep-ph]].

[24] P. Banerjee, S. Borowka, P. K. Dhani, T. Gehrmann and V. Ravindran, JHEP **11** (2018), 130 [arXiv:1809.05388 [hep-ph]].

[25] L. B. Chen, H. T. Li, H. S. Shao and J. Wang, Phys. Lett. B **803** (2020), 135292 [arXiv:1909.06808 [hep-ph]].

[26] L. B. Chen, H. T. Li, H. S. Shao and J. Wang, JHEP **03** (2020), 072 [arXiv:1912.13001 [hep-ph]].

[27] M. Grazzini, G. Heinrich, S. Jones, S. Kallweit, M. Kerner, J. M. Lindert and J. Mazzitelli, JHEP **1805** (2018) 059 doi:10.1007/JHEP05(2018)059 [arXiv:1803.02463 [hep-ph]].

[28] R. Harlander, T. Seidensticker and M. Steinhauser, Phys. Lett. B **426** (1998), 125-132 [arXiv:hep-ph/9712228 [hep-ph]].

[29] T. Seidensticker, [arXiv:hep-ph/9905298 [hep-ph]].

[30] R. N. Lee, arXiv:1212.2685 [hep-ph].

[31] R. N. Lee, J. Phys. Conf. Ser. **523** (2014), 012059 [arXiv:1310.1145 [hep-ph]].

[32] M. Fael, K. Schönwald and M. Steinhauser, [arXiv:2205.03410 [hep-ph]].

[33] P. Nogueira, J. Comput. Phys. **105** (1993), 279-289

[34] B. Ruijl, T. Ueda and J. Vermaseren, arXiv:1707.06453 [hep-ph].

[35] A. V. Smirnov, Comput. Phys. Commun. **189** (2015), 182-191 [arXiv:1408.2372 [hep-ph]].

[36] P. Maierhöfer, J. Usovitsch and P. Uwer, Comput. Phys. Commun. **230** (2018), 99-112 [arXiv:1705.05610 [hep-ph]].

[37] J. Klappert, F. Lange, P. Maierhöfer and J. Usovitsch, Comput. Phys. Commun. **266** (2021), 108024 [arXiv:2008.06494 [hep-ph]].

[38] A. V. Smirnov and V. A. Smirnov, Nucl. Phys. B **960** (2020), 115213 [arXiv:2002.08042 [hep-ph]].

[39] A. V. Kotikov, Phys. Lett. B **254** (1991) 158.

[40] Z. Bern, L. J. Dixon and D. A. Kosower, Nucl. Phys. B **412** (1994), 751-816 [arXiv:hep-ph/9306240 [hep-ph]].

[41] E. Remiddi, Nuovo Cim. A **110** (1997), 1435-1452 [arXiv:hep-th/9711188 [hep-th]].

[42] T. Gehrmann and E. Remiddi, Nucl. Phys. B **580** (2000) 485 [hep-ph/9912329].

[43] J. Klappert and F. Lange, Comput. Phys. Commun. **247** (2020), 106951 [arXiv:1904.00009 [cs.SC]].

[44] J. Klappert, S. Y. Klein and F. Lange, Comput. Phys. Commun. **264** (2021), 107968 [arXiv:2004.01463 [cs.MS]].

[45] G. Mishima, JHEP **02** (2019), 080 [arXiv:1812.04373 [hep-ph]].

[46] M. Beneke and V. A. Smirnov, Nucl. Phys. B **522** (1998) 321 [hep-ph/9711391].

[47] V. A. Smirnov, Springer Tracts Mod. Phys. **177** (2002), 1-262

[48] H.R.P. Ferguson and D.H. Bailey, RNR Technical Report, RNR-91-032; H.R.P. Ferguson, D.H. Bailey and S. Arno, NASA Technical Report, NAS-96-005.

[49] A. V. Smirnov, N. D. Shapurov and L. I. Vysotsky, [arXiv:2110.11660 [hep-ph]].

[50] A. Pak and A. Smirnov, Eur. Phys. J. C **71** (2011) 1626 [arXiv:1011.4863 [hep-ph]].

[51] V. A. Smirnov, Phys. Lett. B **460** (1999), 397-404 [arXiv:hep-ph/9905323 [hep-ph]].

[52] J. B. Tausk, Phys. Lett. B **469** (1999), 225-234 [arXiv:hep-ph/9909506 [hep-ph]].

[53] https://www.ttp.kit.edu/preprints/2022/ttp22-041/.

[54] B. Agarwal, S. P. Jones and A. von Manteuffel, JHEP **05** (2021), 256 [arXiv:2011.15113 [hep-ph]].

[55] S. Borowka, G. Heinrich, S. P. Jones, M. Kerner, J. Schlenk and T. Zirke, Comput. Phys. Commun. **196** (2015) 470 [arXiv:1502.06595 [hep-ph]].

[56] M. Czakon, Comput. Phys. Commun. **175** (2006) 559 [hep-ph/0511200].

[57] J. Ablinger, J. Blümlein, S. Klein and C. Schneider, Nucl. Phys. Proc. Suppl. **205-206** (2010) 110 [arXiv:1006.4797 [math-ph]]; J. Blümlein, A. Hasselhuhn and C. Schneider, PoS (RADCOR 2011) 032 [arXiv:1202.4303 [math-ph]]; C. Schneider, J. Phys. Conf. Ser. **523** (2014) 012037 [arXiv:1310.0160 [cs.SC]].

[58] J. Vermaseren, Int. J. Mod. Phys. A **14** (1999), 2037-2076 [arXiv:hep-ph/9806280 [hep-ph]]; J. Blümlein, Comput. Phys. Commun. **180** (2009), 2218-2249 [arXiv:0901.3106 [hep-ph]]; J. Ablinger, Diploma Thesis, J. Kepler University Linz, 2009, arXiv:1011.1176 [math-ph]; J. Ablinger, J. Blümlein and C. Schneider, J. Math. Phys. **52** (2011) 102301 [arXiv:1105.6063 [math-ph]]; J. Ablinger, J. Blümlein and C. Schneider, J. Math. Phys. **54** (2013), 082301 [arXiv:1302.0378 [math-ph]]; J. Ablinger, Ph.D. Thesis, J. Kepler University Linz, 2012, arXiv:1305.0687 [math-ph]; J. Ablinger, J. Blümlein and C. Schneider, J. Phys. Conf. Ser. **523** (2014), 012060 [arXiv:1310.5645 [math-ph]]; J. Ablinger, J. Blümlein, C. Raab and C. Schneider, J. Math. Phys. **55** (2014), 112301 [arXiv:1407.1822 [hep-th]]; J. Ablinger, PoS **LL2014** (2014), 019 [arXiv:1407.6180 [cs.SC]]; J. Ablinger, [arXiv:1606.02845 [cs.SC]]; J. Ablinger, PoS **RADCOR2017** (2017), 069 [arXiv:1801.01039 [cs.SC]]; J. Ablinger, PoS **LL2018** (2018), 063; J. Ablinger, [arXiv:1902.11001 [math.CO]].

[59] C. Schneider, Sém. Lothar. Combin. **56** (2007) 1, article B56b; C. Schneider, in: Computer Algebra in Quantum Field Theory: Integration, Summation and Special Functions Texts and Monographs in Symbolic Computation eds. C. Schneider and J. Blümlein (Springer, Wien, 2013) 325 arXiv:1304.4134 [cs.SC].

[60] E. Remiddi and J. A. M. Vermaseren, Int. J. Mod. Phys. A **15** (2000) 725 [hep-ph/9905237].

[61] S. Weinzierl, J. Math. Phys. **45** (2004), 2656-2673 [arXiv:hep-ph/0402131 [hep-ph]].

[62] J. Ablinger, J. Blümlein, C. G. Raab and C. Schneider, J. Math. Phys. **55** (2014), 112301 [arXiv:1407.1822 [hep-th]].

[63] J. Ablinger, J. Blümlein and C. Schneider, J. Math. Phys. **52** (2011), 102301 [arXiv:1105.6063 [math-ph]].

[64] J. M. Henn, A. V. Smirnov and V. A. Smirnov, Nucl. Phys. B **919** (2017), 315-324 [arXiv:1512.08389 [hep-th]].

[65] V. A. Smirnov and O. L. Veretin, Nucl. Phys. B **566** (2000) 469 [hep-ph/9907385].

[66] Z. Bern, L. J. Dixon and V. A. Smirnov, Phys. Rev. D **72** (2005) 085001 [hep-th/0505205].

[67] D. Kosower, `https://mbtools.hepforge.org/`

[68] A. Denner, Fortsch. Phys. **41** (1993), 307-420 [arXiv:0709.1075 [hep-ph]].

[69] B. A. Kniehl, J. H. Piclum and M. Steinhauser, Nucl. Phys. B **695** (2004), 199-216 [arXiv:hep-ph/0406254 [hep-ph]].

[70] S. Dittmaier and H. Rzehak, [arXiv:2203.07236 [hep-ph]].

[71] J. Davies, G. Mishima, M. Steinhauser and D. Wellmann, JHEP **04** (2020), 024 [arXiv:2002.05558 [hep-ph]].

[72] L. Chen, J. Davies, G. Heinrich, S. P. Jones, M. Kerner, G. Mishima, J. Schlenk and M. Steinhauser, [arXiv:2204.05225 [hep-ph]].

[73] D. Wellmann, "Top Quark Mass Effects in Higgs and Z Boson Pair Production and Higgs Boson Decays,", PhD thesis, KIT, 2020.